Journal of Nuclear Medicine, published on June 28, 2019 as doi:10.2967/jnumed.119.229393

Preclinical evaluation of $^{203/212}$Pb-labeled low-molecular-weight compounds for targeted radiopharmaceutical therapy of prostate cancer

Sangeeta Ray Banerjee[1,2], Il Minn[1], Vivek Kumar[1], Anders Josefsson[1], Ala Lisok[1], Mary Brummet[1], Jian Chen[1], Ana P. Kiess[2], Kwamena Baidoo[3], Cory Brayton[4], Ronnie C. Mease[1,2], Martin Brechbiel[3], George Sgouros[1], Robert F. Hobbs[1], Martin G. Pomper[1,2]

[1]Russell H. Morgan Department of Radiology and Radiological Science; [2]Sidney Kimmel Comprehensive Cancer Center; [4]Department of Pathology, Johns Hopkins University, School of Medicine Baltimore, MD, USA

[3]National Institutes of Health, Bethesda, MD, USA

Address correspondence to: Sangeeta Ray Banerjee (sray9@jhmi.edu)

Key words: α-particle, theranostic pair, prostate-specific membrane antigen, murine pharmacokinetics, lead-212

ABSTRACT

Targeted radiopharmaceutical therapy (TRT) employing α-particle radiation is a promising approach for treating both large and micrometastatic lesions. We developed prostate-specific membrane antigen (PSMA)-targeted low-molecular-weight (LMW) agents for ^{212}Pb-based TRT of patients with prostate cancer (PC) by evaluating the matching γ-emitting surrogate, ^{203}Pb. Methods: Five rationally designed LMW ligands (L1-L5) were synthesized using the lysine-urea-glutamate (Lys-urea-Glu) scaffold and PSMA inhibition constants (K_i) were determined. Tissue biodistribution and SPECT/CT imaging of ^{203}Pb-L1-^{203}Pb-L5 were performed in mice bearing PSMA(+) PC3 PIP and PSMA(-) PC3 flu flank xenografts. Radiation absorbed dose of the corresponding ^{212}Pb-labeled analogs was determined using the biodistribution data. Antitumor efficacy of ^{212}Pb-L2 was evaluated in PSMA(+) PC3 PIP and PSMA(-) PC3 flu tumor models and in the PSMA(+) luciferase-expressing micrometastatic model. ^{212}Pb-L2 was also evaluated for dose-escalated, long-term toxicity. Results: All new ligands were obtained in high yield and purity. PSMA inhibitory activities ranged from 0.1–17 nM. ^{203}Pb-L1-^{203}Pb-L5 were synthesized in high radiochemical yield and specific activity. Whole-body clearances of ^{203}Pb-L1-^{203}Pb-L5 were fast, the absorbed dose coefficients [mGy/kBq], of the tumor and kidneys were highest for ^{203}Pb-L5 (31.0, 15.2), and lowest for ^{203}Pb-L2 (8.0, 4.2). The tumor-to-kidney absorbed dose ratio was higher for ^{203}Pb-L3 (3.2) and ^{203}Pb-L4 (3.6) compared to the other agents, however, with lower tumor-to-blood ratios. PSMA(+) tumor lesions were visualized through SPECT/CT as early as 0.5 h post-injection. A proof-of-concept therapy study with a single administration of ^{212}Pb-L2 demonstrated dose-dependent inhibition of tumor growth in the PSMA(+) flank tumor model. ^{212}Pb-L2 also demonstrated an increased survival benefit in the micrometastatic model compared to ^{177}Lu-PSMA-617. Long-term toxicity studies in healthy, immunocompetent CD-1 mice revealed kidney as the dose-limiting organ. Conclusions: ^{203}Pb-L1-^{203}Pb-L5 demonstrated favorable pharmacokinetics for ^{212}Pb-based TRT. Antitumor efficacy of ^{212}Pb-L2 supports the corresponding ^{203}Pb/^{212}Pb theranostic pair for PSMA-based α-particle TRT in advanced PC.

INTRODUCTION

Targeted radiopharmaceutical therapy employing α-particles (α-TRT), which causes deposition of ionizing radiation of high-linear energy transfer is accelerating in importance for managing prostate cancer (PC). That is due in part to the unexpected survival benefit conferred by $^{223}RaCl_2$ in patients with bone metastatic castration-resistant prostate cancer (mCRPC) (*1*). Also contributing to that acceleration has been the remarkable decrease in tumor burden demonstrated on images of patients who received ^{225}Ac-PSMA-617 (*2*), which targets PSMA in patients with mCRPC who failed prior, standard treatment (*3,4*). However, salivary and lacrimal gland radiotoxicity may impact the overall survival benefit by reducing quality of life (*5*). As an alternative to ^{225}Ac ($t_{1/2}$=10 d), ^{212}Pb ($t_{1/2}$=10.6 h), which has a shorter physical half-life, is a promising source of a α-emissions that has proved safe and effective in both preclinical models and clinical studies for several indications (*6-9*). ^{212}Pb is commercially available from a ^{224}Ra generator and has well-described radiochemistry (*10*). It is a β-emitter but serves as an *in vivo* nanogenerator of ^{212}Bi ($t_{1/2}$=1.01 h) which decays with an α-particle in its decay chain. ^{212}Pb has been successfully used as stand-alone and in combination with chemotherapy using peptides and monoclonal antibodies as targeting vectors (*6,7,11*). While PSMA-based TRT using low-molecular-weight (LMW) agents and monoclonal antibodies is expanding in management of mCRPC, to date this has employed primarily agents that deliver β-emitting payloads (*12,13*). Few preclinical studies describe detailed evaluation of α-TRT (*14-17*).

A challenge of α-TRT is that the administered therapeutic activities are generally insufficient to be imaged for patient-specific dosimetry. For ^{212}Pb preclinical evaluation presents additional challenges due to a high energy γ-emission from a daughter that requires extra shielding. As a surrogate radionuclide ^{203}Pb ($t_{1/2}$=51.9 h, γ=279 keV), is suitable for γ-well counting and SPECT and has been explored to aid development of ^{212}Pb-based α-TRT (*18,19*). A first-in-human study using ^{203}Pb-based PSMA SPECT has recently appeared (*20*).

Here we report preclinical evaluation of a series of ^{203}Pb-labeled LMW agents for PSMA α-TRT. We first re-evaluated our previous lead agent L1 (*21*) as the ^{203}Pb-labeled analog, and then synthesized four new ligands L2-L5 with further alterations to the chelator and inclusion of a 4-bromobenzyl-Lys-urea-Glu targeting moiety. We employed the 4-bromobenzyl derivative of Lys-urea-Glu as the targeting moiety because of the sustained tumor uptake and high efficacy previously demonstrated by ^{125}I-DCIBzL and its short half-life α-emitting analog, ^{211}At-6 ($t_{1/2}$=7.2 h) (*15,22*) (Fig. 1). The goal of this study was to optimize toward an α-emitting agent with decreased off-target radiotoxicity relative to ^{211}At-6 for PSMA-based α-TRT.

MATERIALS AND METHODS

Reagents, Cell Lines and Animal Models

^{203}Pb was obtained from the NIH Clinical Center cyclotron facility by a ^{203}Tl(d,n)/^{203}Pb reaction and purified from the target as previously described (*23*). The ^{212}Pb was obtained from a ^{224}Ra/^{212}Pb generator (Oak Ridge National Laboratories, Oak Ridge, TN). Sublines of the androgen-independent PC3 human PC cell line, originally derived from an advanced androgen independent bone metastasis, were used (*24*). Animal studies were in compliance with the regulations of the Johns Hopkins Animal Care and Use Committee. Six- to 8-week-old male, Nonobese diabetic/Shi-scid/IL-2rgnull (NSG) mice (Johns Hokins Animal Resources Core) were implanted subcutaneously with PSMA(+) PC3 PIP and PSMA(-) PC3 flu cells [2x10^6 in 100 μL of Matrigel, (Corning, NY)] at the forward right and left flanks, respectively.

Chemistry

Ligands L1 (*21*) and L5 (*25*) and intermediates 3 (*24*) and 4 (*25*) were synthesized following our recent reports. Detailed description for L2, L3, L4 and L5 are provided in the Supplemental Data. PSMA binding affinity of the new compounds were determined using a fluorescence-based competitive binding assay reported by our laboratory (15).

Radiolabeling

An acidic solution of $^{203}PbCl_2$ (~25.9 MBq in 100μL) was neutralized with 6 μL of 5M NH_4OAc to obtain pH ~4.5-5.5. A solution (40 μL) of L1-L5 (1 mg/800 μL 0.1 NH_4OAc) was added and the reaction mixture was incubated at 60-65°C for 45 min. An identical procedure was followed for radiosynthesis of each ^{203}Pb-labeled analog. Radiolabeling was nearly quantitative in each case. ^{212}Pb-L2 was synthesized following a literature method (*26*) at the National Cancer Institute and transported to Johns Hopkins for treatment studies.

Biodistribution

Mice bearing PSMA(+) PC3 PIP and PSMA(-) PC3 flu xenografts were injected via the tail vein with ~1.85 MBq of ^{203}Pb-L1-^{203}Pb-L5 (n=4). Competitive inhibition studies were performed using ZJ43 (*27*), a known LMW PSMA inhibitor, added to the ^{203}Pb-L2-^{203}Pb-L5 formulation, and biodistribution studies were performed at 2 h (n=4).

SPECT/CT Imaging

SPECT/CT imaging of ^{203}Pb-L1, ^{203}Pb-L2, ^{203}Pb-L3 and ^{203}Pb-L4 was performed on a X-SPECT device (GammaMedica, Northridge, CA) following a reported method (*24*). Data were reconstructed and fused using commercial software from the vendor. Data were analyzed using AMIRA software (Thermo Fisher Scientific).

Dosimetry

Time activity curves were generated from the murine biodistribution data of the ^{203}Pb-analogs. Normal tissue and tumor absorbed dose coefficients (ADCs) were estimated for the ^{212}Pb-labeled analog after accounting for the α-radiation deposited locally using the mathematical formalism established by the Medical Internal Radiation Dose (*28*). Only the α-emission was considered in the calculations and assumed to be deposited locally (φ=1). Selected human ADCs were estimated by using a standard mouse-to-human conversion formula for time-integrated activities which were then input into OLINDA/EXM (*29*) (See Supplemental Data).

Radiopharmaceutical Therapy with ^{212}Pb-L2

Therapy in the Xenograft Model and Micrometastatic Models. Mice were injected subcutaneously at the upper flank with PSMA(+) PC3 PIP or PSMA(-) PC3 flu cells. Treatments were administered when tumor volume was 60-100 mm^3. Animals (n=5/group) received a single dose of 1.5 and 3.7 MBq of ^{212}Pb-L2 intravenously or were untreated. Tumors were then measured 2–3 times per week until they reached a tumor volume (V_t) that was 10-fold the initial volume (V_0). The probability of reaching 10 times the initial tumor volume was characterized using Kaplan–Meier curves and comparison was performed using the log-rank test. For the PSMA(+) micrometastatic model, mice were injected intravenously with 1×10^6 PC3-ML-Luc-PSMA cells, as previously reported by us (*15*). At 24 h post-injection of the tumor cells, mice (n=5/group) were injected intravenously with 0, 0.7, 1.5, 3.7 MBq of ^{212}Pb-L2 and 37 MBq of ^{177}Lu-PSMA-617. Metastatic tumor progression and survival were monitored by *in vivo* bioluminescence imaging (IVIS Spectrum; Perkin-Elmer).

Determination of Maximum Tolerated Dose (MTD). The MTD was defined as the highest dose at which no animal died or lost more than 20% of its pretreatment weight. Non-tumor-bearing CD-1 mice (Charles River, n=5/group) received intravenous injections of ^{212}Pb-L2 and

were then weighed and inspected twice per week for at least 12 mo. Urinalysis was performed monthly. On sacrifice, animals were evaluated at the Johns Hopkins Phenotyping Core, which obtained a serum metabolic panel, blood counts, and full necropsy.

Statistical Analysis

Statistical analysis was performed using a 2-tailed t test (GraphPad). *P*-values were considered significant if ≤ 0.05.

RESULTS

Synthesis and Radiolabeling

An abbreviated structure-activity relationship study was performed by modifying the chelating agent, linker and targeting scaffold to develop an optimized agent for α-TRT (Fig. 1). Ligands L1 and L2 were synthesized following our previous report (Supplemental Fig. 1A) (*21*). Although DOTA-monoamide was successfully used for a ^{212}Pb-labeled peptide (*6*), considering the unusual stability of Pb-TCMC compounds in an acidic environment (*11,30*), L2-L4 were designed to contain a TCMC chelating agent. L3-L5 were synthesized following a similar route by employing the 4-bromobenzyl derivative of the Glu-urea-Lys scaffold (Supplemental Fig. 2B-2C). ^{203}Pb-labeled compounds (^{203}Pb-L1-^{203}Pb-L5) and ^{212}Pb-L2 were synthesized in >95% yield and were separated from the corresponding non-radiolabeled precursor by high performance liquid chromatography (HPLC) to obtain a pure product with a specific activity of 0.7-1.9 MBq/nmol. Stability of the radiolabeled compounds was determined by incubation in PBS and in 0.1% HSA in PBS (1×) at 37°C up to 72 h showing >95% stability.

In Vivo Evaluation

Tissue Biodistribution. Biodistribution data (expressed in percentage injected dose per gram of tissue, %ID/g) of ^{203}Pb-L1-^{203}Pb-L5 are shown in Fig. 2 and Supplemental Tables 1-5.

^{203}Pb-L1 exhibited high uptake in the PSMA(+) PC3 PIP tumor as early as 1 h and remained high at 4 h and decreased at 24 h post-injection. Unlike ^{203}Pb-L1, ^{203}Pb-L2 demonstrated highest uptake in the PSMA(+) tumor at 2 h, followed by gradual clearance during 4-24 h post-injection. ^{203}Pb-L2 displayed fast clearance from all normal tissues including kidneys and PSMA(+) tumor. Observing the significant change in biodistribution, especially within the PSMA(+) PC3 PIP tumor and the kidneys by simply changing the chelating agent as we previously experienced (*31*), we further investigated radioligands ^{203}Pb-L3 and ^{203}Pb-L4 bearing the same chelating agent, TCMC-Bn-NCS, and ^{203}Pb-L5 bearing the DOTA-monoamide chelating agent. Fig. 3 summarizes the head-to-head comparison of the PSMA(+) tumor and selected tissues of the tested agents. ^{203}Pb-L2 demonstrated significantly lower tumor uptake up to 2 h compared to ^{203}Pb-L1, ^{203}Pb-L3 and ^{203}Pb-L5 (P <0.01). At 4 h, ^{203}Pb-L2 displayed significantly lower tumor uptake compared to all compounds (^{203}Pb-L1 and ^{203}Pb-L4, P <0.001; ^{203}Pb-L3 and ^{203}Pb-L5, P < 0.05). Additionally, at 24 h post-injection, tumor uptake of ^{203}Pb-L2 was significantly lower compared to ^{203}Pb-L1, ^{203}Pb-L3, and ^{203}Pb-L5. There was no significant difference in PSMA(+) tumor uptake between ^{203}Pb-L3 and ^{203}Pb-L4 during the 0.5–24 h time-points. Both ^{203}Pb-L1 and ^{203}Pb-L5 showed significantly higher tumor retention compared to ^{203}Pb-L3 at 24 h.

^{203}Pb-L2-^{203}Pb-L4 with the TCMC chelating agent displayed significantly lower renal uptake during 1–4 h after injection compared to ^{203}Pb-L1 and ^{203}Pb-L5. At 24 h, renal uptake was significantly lower for ^{203}Pb-L2-^{203}Pb-L4 compared to ^{203}Pb-L1 (P<0.001). ^{203}Pb-L5 displayed significantly higher renal uptake at 2 h and remained high compared to ^{203}Pb-L1 during the 4 h-24 h. There was no significant difference in renal uptake between ^{203}Pb-L2, ^{203}Pb-L3 and ^{203}Pb-L4 up to 4 h and a small but significant difference at 24 h only between ^{203}Pb-L2 and ^{203}Pb-L3. Blocking (PSMA binding specificity) studies were performed for ^{203}Pb-L2-^{203}Pb-L5 by co-administration of 50-100 nmol of the known PSMA inhibitor, ZJ43 (*32*), showing significant

blockade in the PSMA(+) PC3 PIP tumor for all agents (Supplemental Fig. 2). Significant renal blockade was observed for all agents, further indicating specificity for PSMA.

Organ Absorbed Doses. Fig. 4 and Supplemental Table 6 provide a selected list of the murine ADC for ^{212}Pb-analogs. Tumors received ADC of 23.1, 8.0, 18.3, 15.0, 31.0 mGy/kBq for ^{212}Pb-L1, ^{212}Pb-L2, ^{212}Pb-L3, ^{212}Pb-L4 and ^{212}Pb-L5, respectively. Kidneys received the highest ADC and followed a similar trend to that of the PSMA(+) tumors with 23.1, 4.4, 5.8, 4.1, 15.2 mGy/kBq for ^{212}Pb-L1, ^{212}Pb-L2, ^{212}Pb-L3, ^{212}Pb-L4 and ^{212}Pb-L5, respectively. The other potential dose-limiting organ was blood, which demonstrated a nearly 2-fold higher ADC for ^{212}Pb-L3 (0.5 mGy/kBq) and ^{212}Pb-L4 (0.4 mGy/kBq) compared to ^{212}Pb-L1 (0.2 mGy/kBq) and ^{212}Pb-L2 (0.1 mGy/kBq). Absorbed doses of other tissues were low, including heart, lung, liver, spleen and muscle. Salivary gland ADC were low, within the range of 0.28-0.35 mGy/kBq for all agents. Therapeutic ratios of PSMA(+) tumor-to-normal organ, were calculated for kidney, blood and salivary glands (Fig. 5 inset). Therapeutic ratios with respect to kidney demonstrated the following trend: ^{212}Pb-L3>^{212}Pb-L4>^{212}Pb-L5>^{212}Pb-L1 ~ ^{212}Pb-L2. With respect to blood the trend was: ^{212}Pb-L1>^{212}Pb-L5>^{212}Pb-L4>^{212}Pb-L3 ~ ^{212}Pb-L2. Therapeutic ratios with respect to salivary glands were in the range of blood indicating kidney as the dose-limiting organ. Estimated human ADCs from OLINDA/EXM, based on mouse-to-human time-integrated activity conversion is listed in Supplemental Table 7.

In Vivo Imaging. SPECT/CT imaging was performed for ^{203}Pb-L1-Pb-L4 for a visual demonstration of *in vivo* pharmacokinetics (Fig. 5). SPECT/CT images during the 0.5-24 h time-frame after administration confirmed high uptake in the PSMA(+) PC3 PIP tumors but not in the PSMA(-) PC3 flu tumors. Also consistent with the biodistribution data, ^{203}Pb-L2, ^{203}Pb-L3 and ^{203}Pb-L4 displayed very low renal uptake compared to ^{203}Pb-L1 at 2 h post-injection. Fast blood

clearance of all agents was also evident from the imaging study. Compared to ^{203}Pb-L4 (short linker), ^{203}Pb-L3, which bears a long linker, displayed high spleen uptake up to 4 h.

Radiopharmaceutical Therapy

Antitumor Effect in the Flank Tumor Model. The treatment effects of ^{212}Pb-L2 on tumor growth rate and body weight of the mice are shown in Fig. 6A-B. A single administration of 1.5 or 3.7 MBq showed significant tumor growth delay only in PSMA(+) tumors (*P*=0.003) compared to other groups, however, slow tumor regrowth was observed after 8 wk. The median time to reach a 10-fold increase from the initial tumor volume ($V_t/V_0 \leq 10$) was 25 and 39 d for the treatment groups bearing with PSMA(+) tumors administered 1.5 and 3.7 MBq, respectively (Fig. 6C). For control groups, untreated PSMA(+) and PSMA(-) tumors reached the 10-fold increase from the initial tumor volume at 13 and 15 d, respectively. The median time for 10-fold tumor increase of the groups with PSMA(-) tumors treated with 1.5 and 3.7 MBq were 7.5 and 16 d.

Antitumor Effect in the PSMA(+) Micrometastatic Model. For the PSMA(+) micrometastatic tumor model, doses were administered 24 h after tumor cell inoculation. At that time, tumors were considered to be clusters of relatively few cells, which should be favorable for the short-range of α-particles, compared to long-range β^--TRT. The efficacy of α-particle emitting ^{212}Pb-L2 (single administration of 0.7, 1.5 and 3.7 MBq) were compared to untreated group and a group treated β-emitting ^{177}Lu-PSMA-617 (37 MBq) (Fig. 6D). No survival benefit was seen for the group treated with ^{177}Lu-PSMA-617 compared to the control group, (median survival time 46 and 47 days respectively), in contrast, the median survival time for the mice administered with ^{212}Pb-L2 (3.7 MBq) was 58 days, demonstrating moderate but significant improvement (*P*=0.002).

In Vivo Toxicity and MTD. Mean body weight and urinalysis data after a single administration of 0.04-3.7 MBq doses are presented in Fig. 7A. The MTD of ^{212}Pb-L2 in

immunocompetent CD-1 mice was 1.5 MBq. Necropsy at 12 mo post-treatment for lower doses (0.74 and 1.5 MBq) showed acceptable changes in hematologic parameters including blood urea nitrogen (24-44 mg/dL) and creatinine (0.3 mg/dL), alanine aminotransferase and aspartate aminotransferase compared to the control group for kidney and liver function, respectively, (Fig. 7B, Supplemental Tables 8-11). Relative kidney mass was comparable for both groups. Histopathologic evaluation revealed moderate nephrotoxicity and tubule epithelial karyomegaly in the treated compared to control animals (Fig. 7C). Atypia within the epithelium of the glomeruli was identified, however, chronic nephropathy with typical degenerative and regenerative changes can be present in obese mice in chronic studies (*33*). No histopathological radiotoxicity was noted in other organs, including bone marrow. Clinically evident toxicity of mice treated with 3.7 MBq was identified at 7 months, including body weight loss, proteinuria, anemia and azotemia in several animals. Those results support the dosimetry that designated kidney as the dose-limiting organ. The projection to human data is simplistic but indicates that activities on the order of 1-3 GBq could be delivered to humans assuming MTD constraints of 23 Gy to kidney and 2 Gy to the bone marrow (Supplemental Table 7).

DISCUSSION

Although encouraging, PSMA-targeted ^{177}Lu-based β^--TRT is not effective in ~30% of patients and is considered unsuitable for patients with diffuse red marrow infiltration (*12*). ^{225}Ac-based α-TRT has been pursued to overcome resistance to β^--TRT as salvage therapy for treatment-refractory mCRPC (*2*). Those clinical investigations have revealed that α-emitters are effective in controlling large lesions in addition to their predicted role in elimination of microscopic disease owing to their short-range of energy deposition as well as a noted bystander or abscopal effect. Several α-emitting isotopes such as ^{213}Bi, ^{211}At, ^{212}Pb and ^{225}Ac have been studied clinically and all of them are being investigated preclinically by us and others in the context of PSMA-based TRT (*15,16,19,20*).

There are several radiobiologic effects that contribute to the superior efficacy of α-emitters relative to β^--emitters, one of which is by activating several unique molecular pathways (*34*). That mechanism of radiotoxicity is independent of tissue oxygenation, dose rate, and cellular resistance to γ- or β^--irradiation and chemotherapy (*35*). Accordingly, normal tissues might also be expected to receive those higher toxic doses causing severe side effects for the α- compared to β^--emitters. A careful evaluation of the absorbed doses from radiosensitive vital organs based on long-term toxicity studies as described in this report may provide reliable dose prediction for an initial phase I dose escalation trial.

The major acute toxicity from clinical PSMA-based α-TRT is related to salivary and lacrimal gland dysfunction (*5*). Although renal toxicity has so far proved minimal for PSMA β^-- and α-TRT (*2,12*), late nephrotoxicity remains a concern as an insubstantial number of patients have been evaluated many years out from therapy. For example, long-term, chronic nephrotoxicity was reported as a major side-effect for patients treated with ^{177}Lu-/Y^{90}-octreotate (*36-38*). The α-emitters, due to their short-range radiation, may actually yield a lower absorbed dose to the radiosensitive glomeruli, however, they are much more potent with respect to promoting damage to the renal tubules (*39*). ^{225}Ac in particular, along with its three α-emitting daughters, is expected to have substantial radiotoxicity due to the redistribution of daughters to the normal organs after each α-decay. It is known that free bismuth is accumulated by the renal cortex (*39*), which is of concern due to the radioactive bismuth daughters of ^{225}Ac.

^{212}Pb offers an alternative for PSMA-based α-TRT owing to its short half-life and its availability through a commercial generator. ^{212}Pb-based α-TRT using LMW agents has not been studied extensively (*6*). The preclinical work described here leveraged several key features of the Lys-Glu-urea scaffold to optimize ^{212}Pb-based α-TRT targeting PSMA. An abbreviated structure-activity relationship study allowed us to modulate off-target toxicity while maintaining

higher tumor radiation absorbed dose. Because of the short half-life of ^{212}Pb, a high dose is expected to be delivered to the kidneys within the first few hours, consequently, we paid careful attention to renal dose. Additionally, we anticipate a lower salivary gland absorbed dose for the ^{212}Pb-labeled compounds compared to ^{225}Ac-labeled compounds because of the short half-life and less complicated dosimetry associated with ^{212}Pb. We recognize that direct comparison of salivary gland absorbed dose for ^{212}Pb- and ^{225}Ac-labeled analogs based on biodistribution data from ^{203}Pb-labeled compounds may be speculative since the studies were performed only out to 24 h post-injection, and the compounds harboring each radioisotope have their own pharmacokinetic properties.

Biodistribution data revealed that the agents with DOTA and DOTA-mono amide chelating agents (^{203}Pb-L1 and ^{203}Pb-L5) tended to display higher renal retention compared to the positively charged agents that carry TCMC as the chelator (^{203}Pb-L2-^{203}Pb-L4). Similarly, higher tumor uptake and retention were observed with ^{203}Pb-L1 and ^{203}Pb-L5 compared to TCMC-chelated agents after 24 h. Among the TCMC-chelated compounds, ^{203}Pb-L2 without a 4-bromobenzyl moiety from the targeting Lys-urea-Glu, displayed significantly faster clearance from the PSMA(+) tumor and normal tissues at all time points. While ^{203}Pb-L3 and ^{203}Pb-L4 demonstrated comparable tumor uptake to ^{203}Pb-L1/^{203}Pb-L5, they displayed significantly lower renal uptake at 4 h. However, the high tumor-to-kidney ratios of ^{203}Pb-L3/^{203}Pb-L4 were offset somewhat by their relatively high blood activity levels at early time-points compared to ^{203}Pb-L1/^{203}Pb-L5. Accordingly, ^{212}Pb-L2 was selected for the proof-of-concept α-TRT.

^{212}Pb-L2 provided significant flank tumor growth delay in the PSMA(+) tumors. The median survival of animals receiving the agent was comparable to ^{211}At-6 (*15*). Significantly, ^{212}Pb-L2 demonstrated ~6-fold lower kidney absorbed dose compared to our previous short half-life α-emitting agent ^{211}At-6 (*15*). Consequently, the MTD observed for a single administered dose

in healthy, immunocompetent CD-1 mice increased from ^{211}At-6, at 37 kBq, to ^{212}Pb-L2, at 1.5 MBq. An administered dose of 3.7 MBq of ^{212}Pb-L2 showed characteristic features of late radiation nephropathy at 7 months post-treatment. In contrast, dose of up to 1.5 MBq induced only discrete, nonspecific changes in the kidney, while still enabling a measure of tumor growth control. To address the late nephropathy issue, we anticipate that a fractionated dose would be more appropriate for this short half-life radioligand. Alternatively, a partial kidney blocking strategy using DCIBzL could be useful for ^{212}Pb-based α-TRT

^{212}Pb-L2 also proved more effective in treating micrometastases compared to β^--emitting ^{177}Lu-PSMA-617 in our PSMA(+) micrometastatic tumor model (*15*). That was most likely due to the superior capability of the high-linear energy radiation of ^{212}Pb in this type of model, and is consistent with previous reports using similar LMW peptides and antibodies (*40-42*). Theoretically, the total energy for each ^{212}Pb disintegration is 6-8 MeV compared to a mean β-radiation energy for each ^{177}Lu disintegration of 0.4 MeV, providing a 15-fold difference. The administered dose ratio for ^{212}Pb:^{177}Lu was 1:10 favored for ^{212}Pb-L2. A higher dose may be allowed for ^{212}Pb-L2, when considering a possible loss of activity after α-emission and also, the half-life of ^{212}Pb-L2 (0.4 d) is much shorter compared to ^{177}Lu (6.7 d).

The high MTDs projected for humans as compared to other α-emitters can be explained by *a)* only one α-emission per ^{212}Pb decay, versus four for ^{225}Ac and ^{223}Ra; *b)* shorter half-life; and *c)* faster normal organ biological clearance. This is also consistent with the murine MTD of 1.85–3.7 MBq, which is in the range of the fractional ^{223}Ra activity administered to humans. Nevertheless, such projections are highly uncertain, and any human application should be carried out in increasing increments from values well below the calculated MTD.

Although ^{212}Pb-L2 displayed a short circulation time within blood and low renal uptake relative to other compounds in this series, long-term renal toxicity for the higher doses is a concern. That is admittedly related to the physical characteristics of ^{212}Pb decay rather than to the *in vivo* stability of the ^{212}Pb-TCMC or ^{212}Pb-DOTA interactions. Beta-particle emission of ^{212}Pb is associated with ɣ-ray emission pathways that competes with internal conversion with 30% efficiency. Internal conversion decay destabilizes resulting bismuth complexes promoting rupture of the Bi-chelator chemical bonds resulting in release of ^{212}Bi, which is known to accumulate mainly in the renal proximal tubules (*11*). Therefore, safety and efficacy of these new ^{212}Pb-based could be further optimized with ex vivo murine studies and small-scale (macro-to-micro) dosimetry with bio-kinetic modeling applied to clinical scenarios (*43*). An additional clinical consideration is that the ^{212}Pb decay chain includes several high energy photons [1.6 MeV (1.5%); 727 keV (6.6%); 785 keV (1.1%); 861 keV (4.5%)], that would possibly require hospitalization for radiation safety reasons.

CONCLUSION

We have evaluated in preclinical models the theranostic radionuclide pair ^{203}Pb/^{212}Pb in a focused series of compounds for PSMA-based α-TRT. ^{212}Pb-L2 demonstrated PSMA-specific tumor growth delay in both large and micrometastatic tumor models. The kidney was identified as the dose-limiting organ from the long-term toxicity study. Future studies are directed toward evaluation of the safety and efficacy of ^{212}Pb-L3-^{212}Pb-L5 studied at the MTD, in comparison with the corresponding long-lived α-emitters, ^{225}Ac-L3-^{225}Ac-L5, as we work toward clinical translation with our optimized, lead compound.

ACKNOWLEDGMENTS

We are grateful for the following sources of support: The Patrick C. Walsh Prostate Cancer Research Fund, P30CA006973, CA151838, CA134675, CA184228, CA183031, EB024495, and the Commonwealth Foundation.

CONFLICTS OF INTEREST

Drs. Banerjee, Minn, Mease and Pomper are co-inventors on one or more U.S. patents covering compounds discussed in this submission and as such is entitled to a portion of any licensing fees and royalties generated by this technology. This arrangement has been reviewed and approved by the Johns Hopkins University in accordance with its conflict-of-interest policies. No other potential conflicts of interest relevant to this article exist.

Key Points: QUESTION: Do PSMA-targeted α-emitting ^{212}Pb-labeled low-molecular weight radioligands display required safety and efficacy in preclinical studies for potential clinical translation as an alternative to long half-life ^{225}Ac-based therapy with reduced off-target effect? PERTINENT FINDINGS: Our report has addressed the question by taking strategic preclinical research.

1. We generated five ^{212}Pb-labeled PSMA-targeted compounds and chose a lead among them, ^{212}Pb-L2, which demonstrated tumor growth control in both flank and micrometastatic models with the lowest off-target effects in this series
2. We determined the MTD of ^{212}Pb-L2 in healthy, immunocompetent mice to be 1.5 MBq to inform a future phase I clinical trial.

REFERENCES

1. Parker C, Nilsson S, Heinrich D, et al. Alpha emitter radium-223 and survival in metastatic prostate cancer. *N Engl J Med.* 2013;369:213-223.

2. Kratochwil C, Bruchertseifer F, Rathke H, et al. Targeted alpha therapy of mCRPC with ^{225}Actinium-PSMA-617: Dosimetry estimate and empirical dose finding. *J Nucl Med.* 2017;58:1624-1631.

3. Zukotynski KA, Valliant J, Bénard F, et al. Flare on serial prostate-specific membrane antigen–targeted ^{18}F-DCFPyL PET/CT examinations in castration-resistant prostate cancer: first observations. *Clin Nucl Med.* 2018;43:213-216.

4. Afshar-Oromieh A, Debus N, Uhrig M, et al. Impact of long-term androgen deprivation therapy on PSMA ligand PET/CT in patients with castration-sensitive prostate cancer. *Eur J Nucl Med Mol Imaging.* 2018;45:2045-2054.

5. Langbein T, Chaussé G, Baum RP. Salivary gland toxicity of PSMA radioligand therapy: relevance and preventive strategies. *J Nucl Med.* 2018;59:1172-1173.

6. Miao Y, Hylarides M, Fisher DR, et al. Melanoma therapy via peptide-targeted α-radiation. *Clin Cancer Res.* 2005;11:5616-5621.

7. Milenic DE, Garmestani K, Brady ED, et al. Potentiation of high-LET radiation by gemcitabine: targeting HER2 with trastuzumab to treat disseminated peritoneal disease. *Clin Cancer Res.* 2007;13:1926-1935.

8. Meredith RF, Torgue J, Azure MT, et al. Pharmacokinetics and imaging of ^{212}Pb-TCMC-trastuzumab after intraperitoneal administration in ovarian cancer patients. *Cancer Biother Radiopharm.* 2014;29:12-17.

9. Meredith R, Torgue J, Shen S, et al. Dose escalation and dosimetry of first-in-human α radioimmunotherapy with ^{212}Pb-TCMC-Trastuzumab. *J Nucl Med.* 2014;55:1636-1642.

10. Atcher RW, Friedman AM, Hines JJ. An improved generator for the production of ^{212}Pb and ^{212}Bi from ^{224}Ra. *Int J Rad Appl Instrum A.* 1988;39:283-286.

11. Yong K, Brechbiel MW. Towards translation of ^{212}Pb as a clinical therapeutic; getting the lead in! *Dalton Trans.* 2011;40:6068-6076.

12. Rahbar K, Ahmadzadehfar H, Kratochwil C, et al. German multicenter study investigating ^{177}Lu-PSMA-617 radioligand therapy in advanced prostate cancer patients. *J Nucl Med.* 2017;58:85-90.

13. Hofman MS, Violet J, Hicks RJ, et al. ^{177}Lu-PSMA-617 radionuclide treatment in patients with metastatic castration-resistant prostate cancer (LuPSMA trial): a single-centre, single-arm, phase 2 study. *Lancet Oncol.* 2018;19:825-833.

14. McDevitt MR, Barendswaard E, Ma D, et al. An alpha-particle emitting antibody ([^{213}Bi]J591) for radioimmunotherapy of prostate cancer. *Cancer Res.* 2000;60:6095-6100.

15. Kiess AP, Minn I, Vaidyanathan G, et al. (2S)-2-(3-(1-Carboxy-5-(4-211At-Astatobenzamido)Pentyl)Ureido)-Pentanedioic acid for PSMA-targeted alpha-particle radiopharmaceutical therapy. *J Nucl Med* 2016;57:1569-1575.

16. Kelly JM, Amor-Coarasa A, Ponnala S, et al. A single dose of ^{225}Ac-RPS-074 induces a complete tumor response in an lncap xenograft model. *J Nucl Med.* 2019;60:649-655.

17. Nonnekens J, Chatalic KL, Molkenboer-Kuenen JD, et al. ^{213}Bi-Labeled Prostate-Specific Membrane Antigen-targeting agents induce DNA double-strand breaks in prostate cancer xenografts. *Cancer Biother Radiopharm.* 2017;32:67-73.

18. Miao Y, Figueroa SD, Fisher DR, et al. Lead-203-labeled alpha-melanocyte stimulating hormone peptide as an imaging probe for melanoma detection. *J Nucl Med* 2008;49:823-829.

19. Ray S, Kumar V, Lisok A, et al. Low and high LET radiometal-based therapeutics for prostate caner. *J Nucl Med.* 2017;58:312.

20. dos Santos JC, Schäfer M, Bauder-Wüst U, et al. Development and dosimetry of ^{203}Pb/^{212}Pb-labelled PSMA ligands: bringing “the lead” into PSMA-targeted alpha therapy? *Eur J Nucl Med Mol Imaging.* 2019.

21. Banerjee SR, Foss CA, Pullambhatla M, et al. Preclinical evaluation of ^{86}Y-labeled inhibitors of prostate-specific membrane antigen for dosimetry estimates. *J Nucl Med.* 2015;56:628-634.

22. Chen Y, Foss CA, Byun Y, et al. Radiohalogenated prostate-specific membrane antigen (PSMA)-based ureas as imaging agents for prostate cancer. *J Med Chem.* 2008;51:7933-7943.

23. Garmestani K, Milenic DE, Brady ED, Plascjak PS, Brechbiel MW. Purification of cyclotron-produced ^{203}Pb for labeling Herceptin. *Nucl Med Biol.* 2005;32:301-305.

24. Banerjee SR, Pullambhatla M, Byun Y, et al. Sequential SPECT and optical imaging of experimental models of prostate cancer with a dual modality inhibitor of the prostate-specific membrane antigen. *Angew Chem Int Ed.* 2011;50:9167-9170.

25. Banerjee SR, Kumar V, Lisok A, et al. ^{177}Lu-Labeled low-molecular-weight agents for PSMA-targeted radiopharmaceutical therapy. *Eur J Nucl Med Mol imaging.* 2019.

26. Baidoo KE, Milenic DE, Brechbiel MW. Methodology for labeling proteins and peptides with lead-212 (212Pb). *Nucl Med Biol.* 2013;40:592-599.

27. Yamamoto T, Saito O, Aoe T, et al. Local administration of N-acetylaspartylglutamate (NAAG) peptidase inhibitors is analgesic in peripheral pain in rats. *Eur J Neurosci.* 2007;25:147-158.

28. Bolch WE, Eckerman KF, Sgouros G, Thomas SR. MIRD Pamphlet No. 21: A Generalized schema for radiopharmaceutical dosimetry—standardization of nomenclature. *J Nucl Med.* 2009;50:477-484.

29. Stabin MG, Sparks RB, Crowe E. OLINDA/EXM: the second-generation personal computer software for internal dose assessment in nuclear medicine. *J Nucl Med.* 2005;46:1023-1027.

30. Chappell LL, Dadachova E, Milenic DE, Garmestani K, Wu C, Brechbiel MW. Synthesis, characterization, and evaluation of a novel bifunctional chelating agent for the lead isotopes ^{203}Pb and ^{212}Pb. *Nucl Med Biol.* 2000;27:93-100.

31. Ray Banerjee S, Pullambhatla M, Foss CA, et al. Effect of chelators on the pharmacokinetics of ^{99m}Tc-labeled imaging agents for the prostate-specific membrane antigen (PSMA). *J Med Chem.* 2013;56:6108-6121.

32. Yamamoto T, Saito O, Aoe T, et al. Local administration of N-acetylaspartylglutamate (NAAG) peptidase inhibitors is analgesic in peripheral pain in rats. *Eur J Neursci.* 2007;25:147-158.

33. National Toxicology Program. Kidney. https://ntp.niehs.nih.gov/nnl/urinary/kidney/index.htm. Updated October 28, 2014, Accessed June 14, 2019.

34. Baidoo KE, Yong K, Brechbiel MW. Molecular pathways: targeted α-particle radiation therapy. *Clin Cancer Res.* 2013;19:530-537.

35. Sgouros GE. MIRD monograph: radiobiology and dosimetry for radiopharmaceutical therapy with alpha-particle emitters. Reston, VA: Soc. Nucl. Med. Mol. Imaging. 2015

36. Bodei L, Kidd M, Paganelli G, et al. Long-term tolerability of PRRT in 807 patients with neuroendocrine tumours: the value and limitations of clinical factors. *Eur J Nucl Med Mol Imaging.* 2015;42:5-19.

37. Gabriel M, Nilica B, Kaiser B, Virgolini IJ. Twelve-year follow-up after peptide receptor radionuclide therapy (PRRT). *J Nucl Med.* 2018;60:524-529.

38. Bergsma H, Konijnenberg MW, van der Zwan WA, et al. Nephrotoxicity after PRRT with ^{177}Lu-DOTA-octreotate. *Eur J Nucl Med Mol imaging.* 2016;43:1802-1811.

39. Miederer M, McDevitt MR, Sgouros G, Kramer K, Cheung N-KV, Scheinberg DA. Pharmacokinetics, dosimetry, and toxicity of the targetable atomic generator, ^{225}Ac-hum195, in nonhuman primates. *J Nucl Med.* 2004;45:129-137.

40. Wild D, Frischknecht M, Zhang H, et al. Alpha- versus beta-particle radiopeptide therapy in a human prostate cancer model (^{213}Bi-DOTA-PESIN and ^{213}Bi-AMBA versus ^{177}Lu-DOTA-PESIN). *Cancer Res.* 2011;71:1009-1018.

41. Miederer M, Henriksen G, Alke A, et al. Preclinical evaluation of the alpha-particle generator nuclide 225Ac for somatostatin receptor radiotherapy of neuroendocrine tumors. *Clin Cancer Res.* 2008;14:3555-3561.

42. Song H, Hobbs RF, Vajravelu R, et al. Radioimmunotherapy of breast cancer metastases with alpha-particle emitter ^{225}Ac: comparing efficacy with ^{213}Bi and ^{90}Y. *Cancer Res.* 2009;69:8941-8948.

43. Hobbs RF, Song H, Huso DL, Sundel MH, Sgouros G. A nephron-based model of the kidneys for macro-to-micro alpha-particle dosimetry. *Phys Med Biol.* 2012;57:4403-4424.

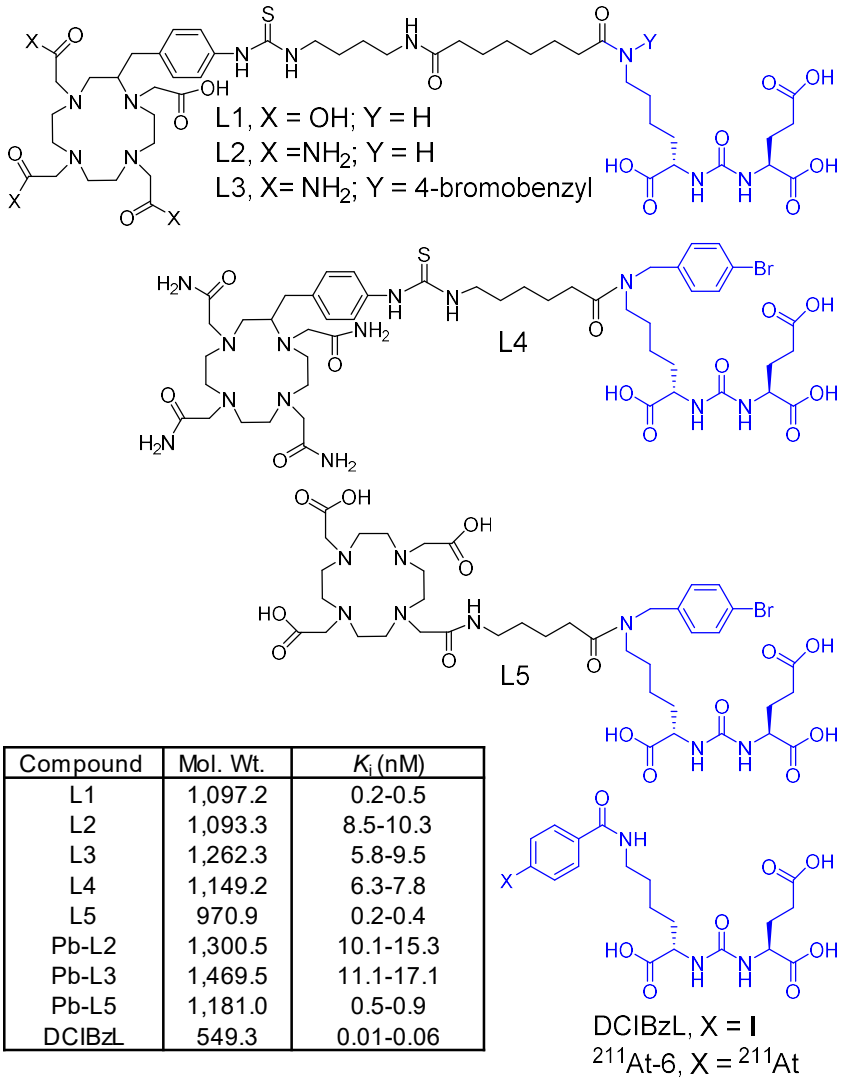

Compound	Mol. Wt.	K_i (nM)
L1	1,097.2	0.2-0.5
L2	1,093.3	8.5-10.3
L3	1,262.3	5.8-9.5
L4	1,149.2	6.3-7.8
L5	970.9	0.2-0.4
Pb-L2	1,300.5	10.1-15.3
Pb-L3	1,469.5	11.1-17.1
Pb-L5	1,181.0	0.5-0.9
DCIBzL	549.3	0.01-0.06

Figure 1. Structures of DCIBzL, ^{211}At-6 and ligands L1-L5, for $^{203/212}$Pb-labeled PSMA-targeted α-particle theranostics. Molecular weight and PSMA inhibition constant (K_i) of the new compounds are listed in the inset table.

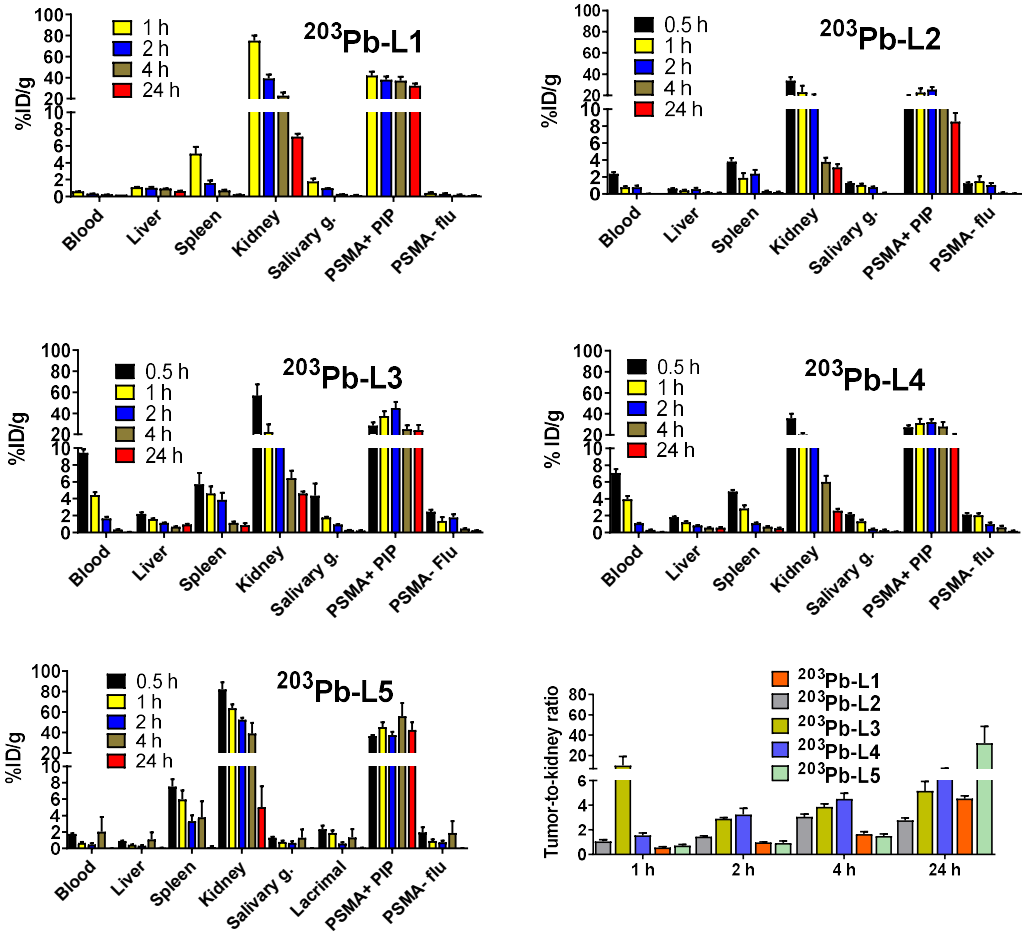

Figure 2. Tissue biodistribution in mice bearing PSMA(+) PC3 PIP and PSMA(-) PC3 flu tumors on either flank (n=4) and tumor-to-normal organ ratios.

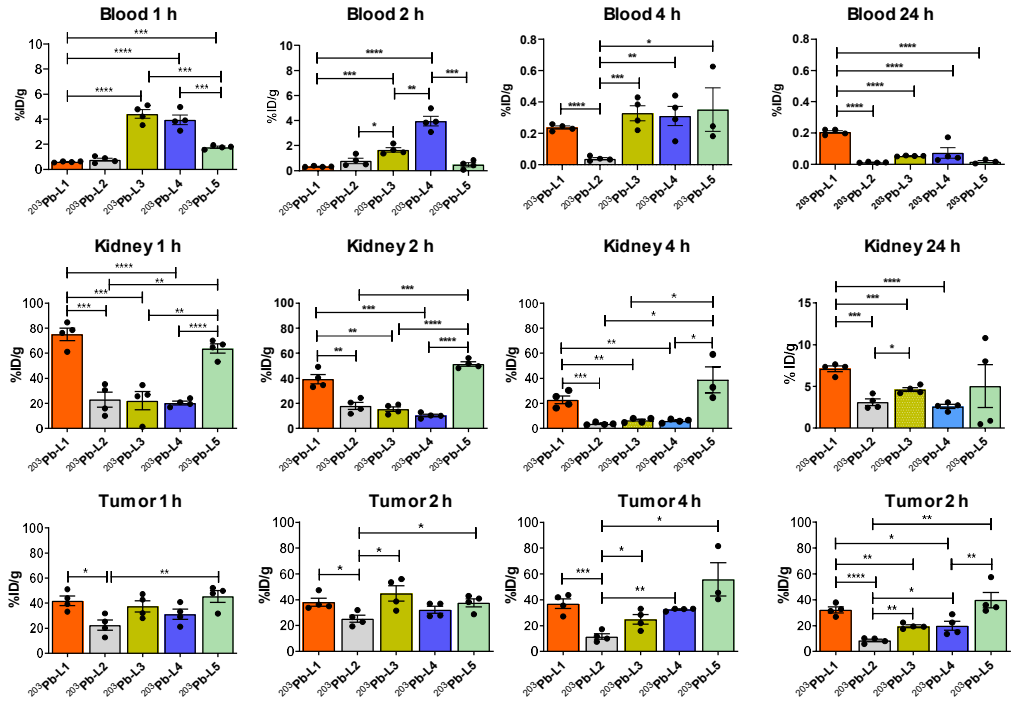

Figure 3. Time-dependent uptake of ^{203}Pb-L1-^{203}Pb-L5 in selected tissues. **** P<0.0001, *** P<0.001, ** P< 0.01, * P<0.05

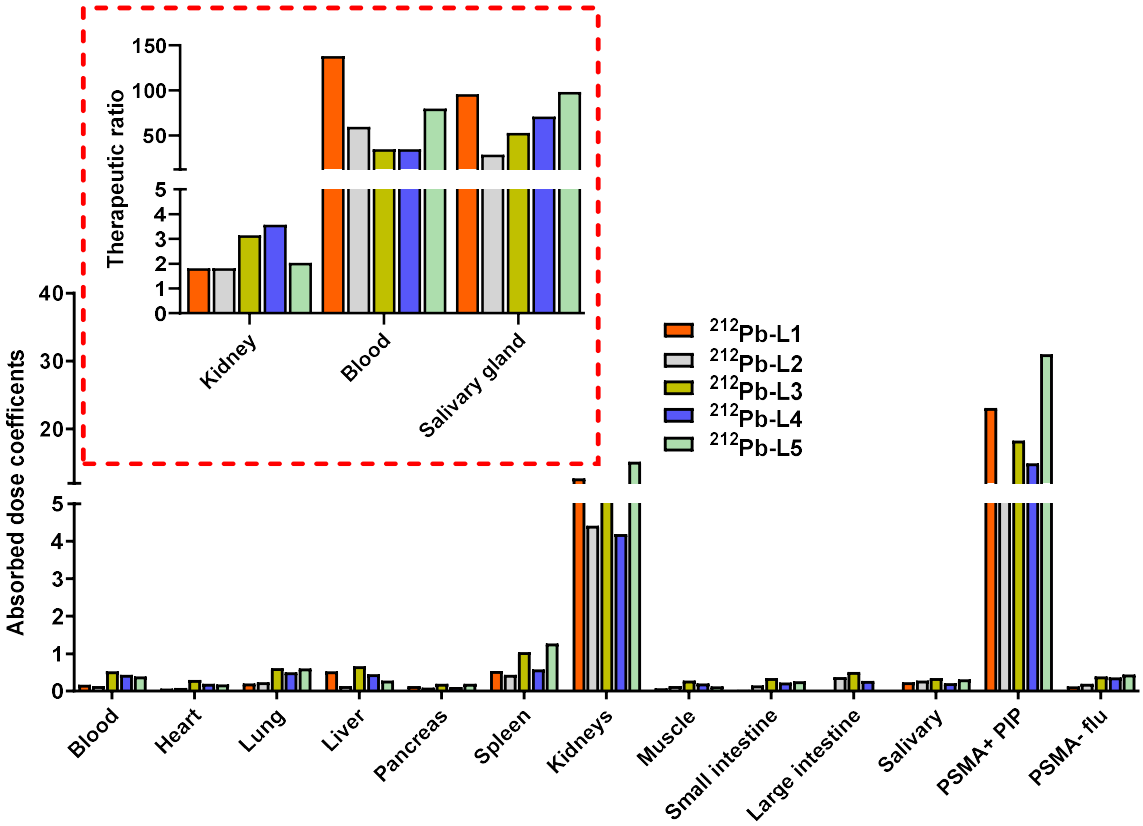

Figure 4. Estimated absorbed dose coefficients (mGy/kBq). Inset showing therapeutic ratio, calculated as absorbed dose coefficients of tumor-to-blood (Blood), tumor-to-kidney (Kidney) and tumor-to-salivary glands (Salivary glands).

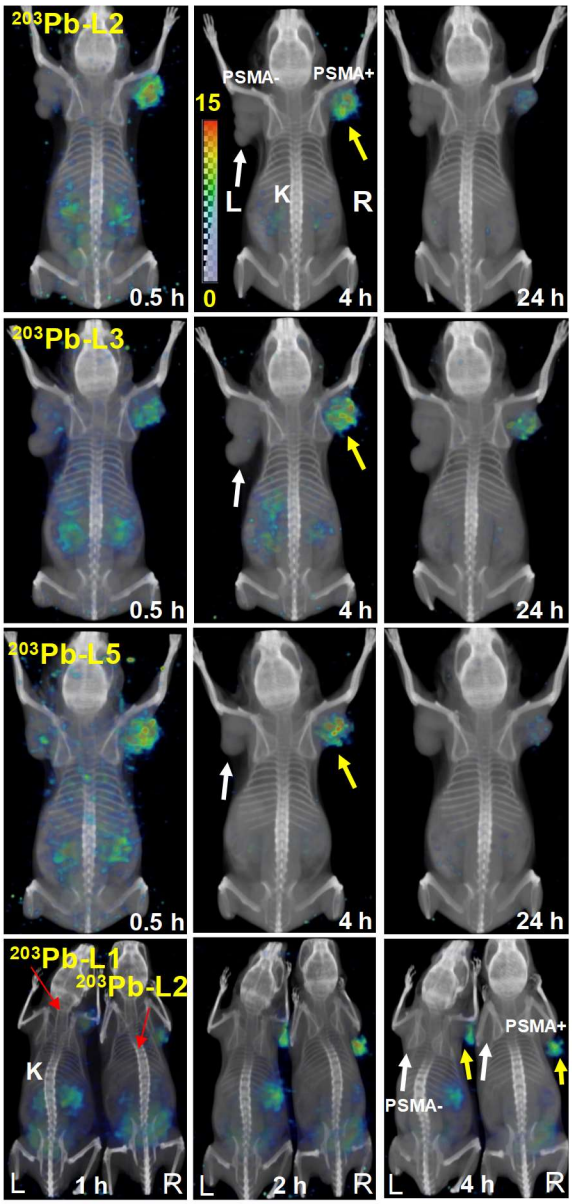

Figure 5. Whole-body volume rendering SPECT/CT in mice bearing PSMA(+) PC3 PIP and PSMA(-) PC3 flu tumors. Mice were injected intravenously ~26 MBq showing the uptake only in PSMA(+) PC3 PIP tumor and kidneys. White arrow - PSMA(-) PC3 flu tumor; yellow arrow - PSMA(+) PIP tumors; K = kidney.

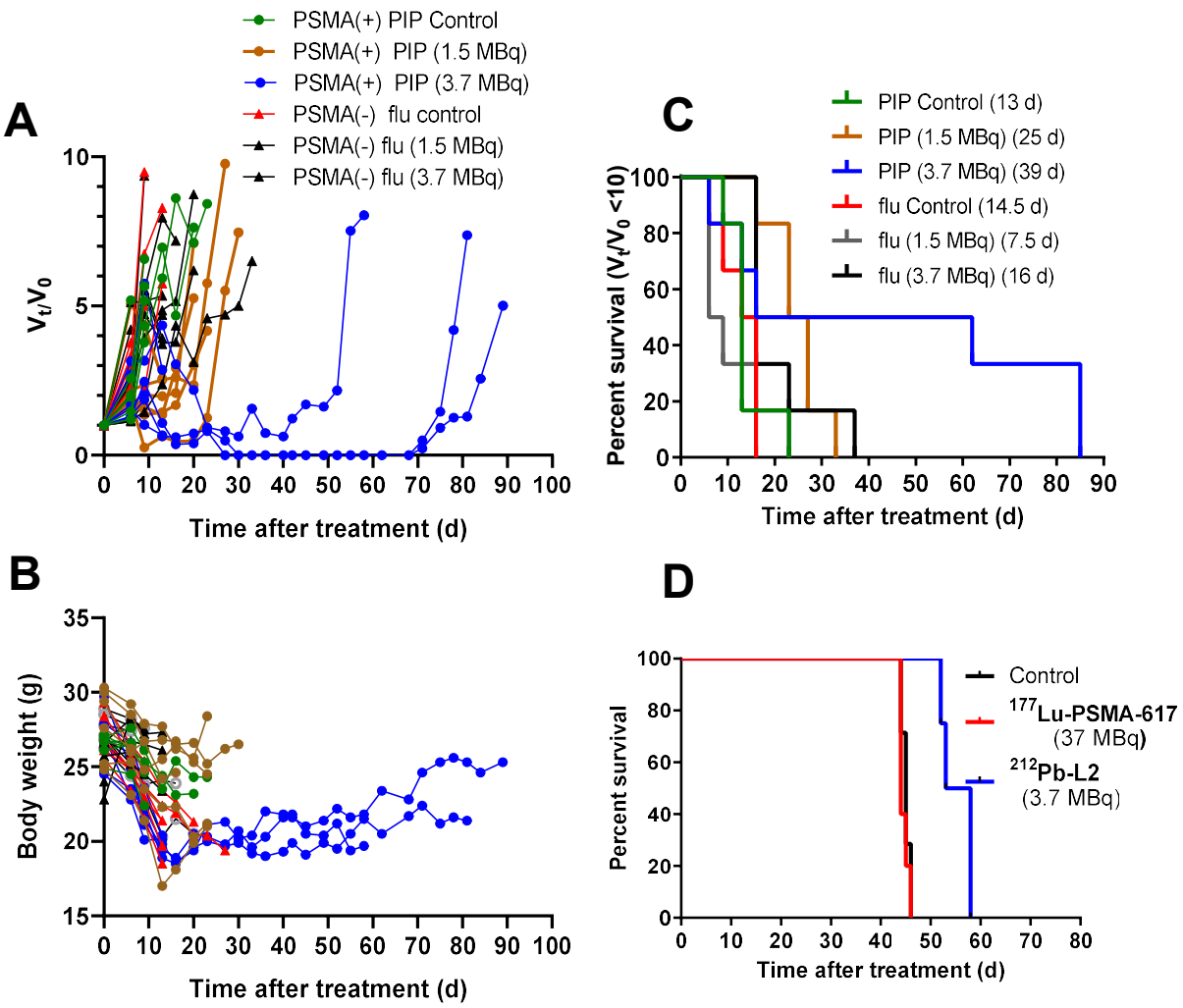

Figure 6. Treatment effect of ^{212}Pb-L2. A. Ratio of tumor volume (V_t/V_0) changes upon treatment with single administration (n=5). Each line represents one mouse; B. Changes in body weight of the corresponding treatment group. Dose and median time for (V_t/V_0)=10 are in the parenthesis; C. Kaplan–Meier curve illustrating time to grow 10-fold in tumor volume after treatment with single-administration of ^{212}Pb-L2 or control. B. Kaplan–Meier curve showing significant improvement in survival after treatment in micrometastatic model compared to control and ^{177}Lu-PSMA-617.

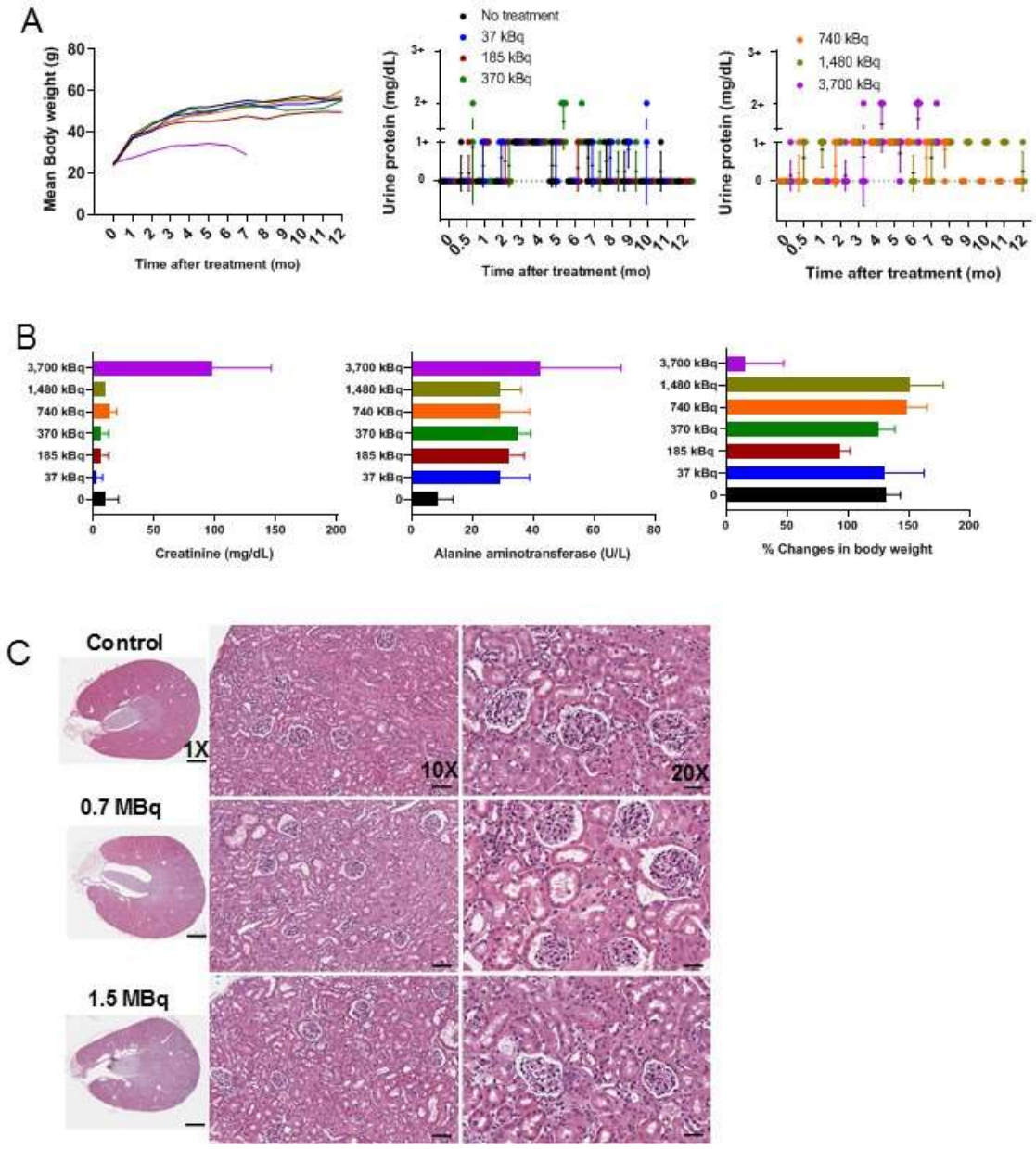

Figure 7. Analysis of radiotoxicity parameters after single-administration of ^{212}Pb-L2 in healthy CD-1 mice (n=5) for 1-12 months. A. Mean body weight and urine protein level measured by dipstick showed dose-dependent proteinuria occurring in the 3.7 MBq treatment group. A different batch of mice (n=7) for the treatment group administered with 3.7 MBq. Urine protein (trace, 0-10 mg/dL; 1+, 30 mg/dL; 2+,100 mg/dL). Each dot represents urine protein value for each mouse; B. The creatinine concentration and alanine aminotransferase in the serum;

percent of body weight changes of mice at 13 months after injection; all measurements for 3.7 MBq treatment group was done at 7 months after injections. C. Hematoxylin and Eosin staining of kidneys from nontreated mouse (A) and mouse treated with 0.7 and 1.5 MBq of ^{212}Pb-L2 (B and C) after 12 months showing mild tubular damage and regenerative and degenerative changes in the proximal tubules (scale bar 50 μm, 20X).

Supplemental Figure 1. A. Synthetic routes for ligands **L2** and **L3**. **B**. Synthetic scheme for the intermediate compound **4**. **C**. Synthetic schemes for ligand **L4** and **L5** and representative radiolabeling scheme of ^{203}**Pb-L4**.

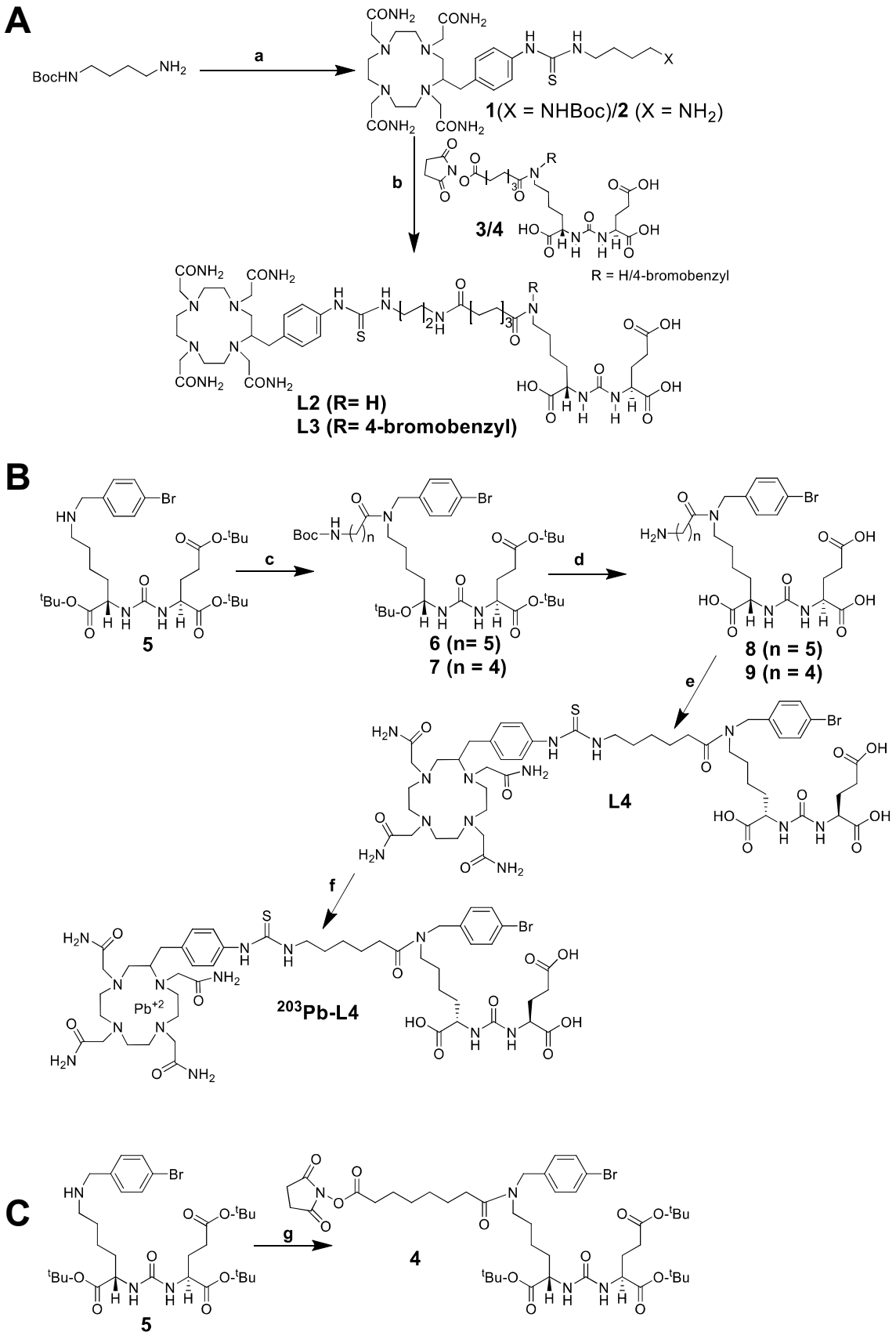

a. (i) DOTA-Bn-SCN, DMSO, Et_3N, 40°C, 4 h; (ii) TFA:CH_2Cl_2 (1:1), rt, 2 h; **b**. DMSO, DIEA, rt, 2h; **c.** 6-(Boc-amino)hexanoic acid, DIPEA,TSTU, DMF, rt, 4 h; **d.** TFC:CH_2Cl_2 (1:1), rt, 2 h; **e.** TCMC-Bn-SCN, DMSO, DIPEA, rt; **f.** $Pb(NO_3)_2$, 0.2 M NaOAc, pH ~4-5.5, 40-50°C; **g.** Disuccinimidyl suberate, Et_3N, DMF, rt, 2 h.

Supplemental Figure 2. PSMA binding specificity of the compounds were assessed by co-administration of ^{203}Pb-L2-^{203}Pb-L5 with 50 nmol of ZJ43 for ^{203}Pb-L2, ^{203}Pb-L3 and ^{203}Pb-L4 and 100 nmol for ^{203}Pb-L5.

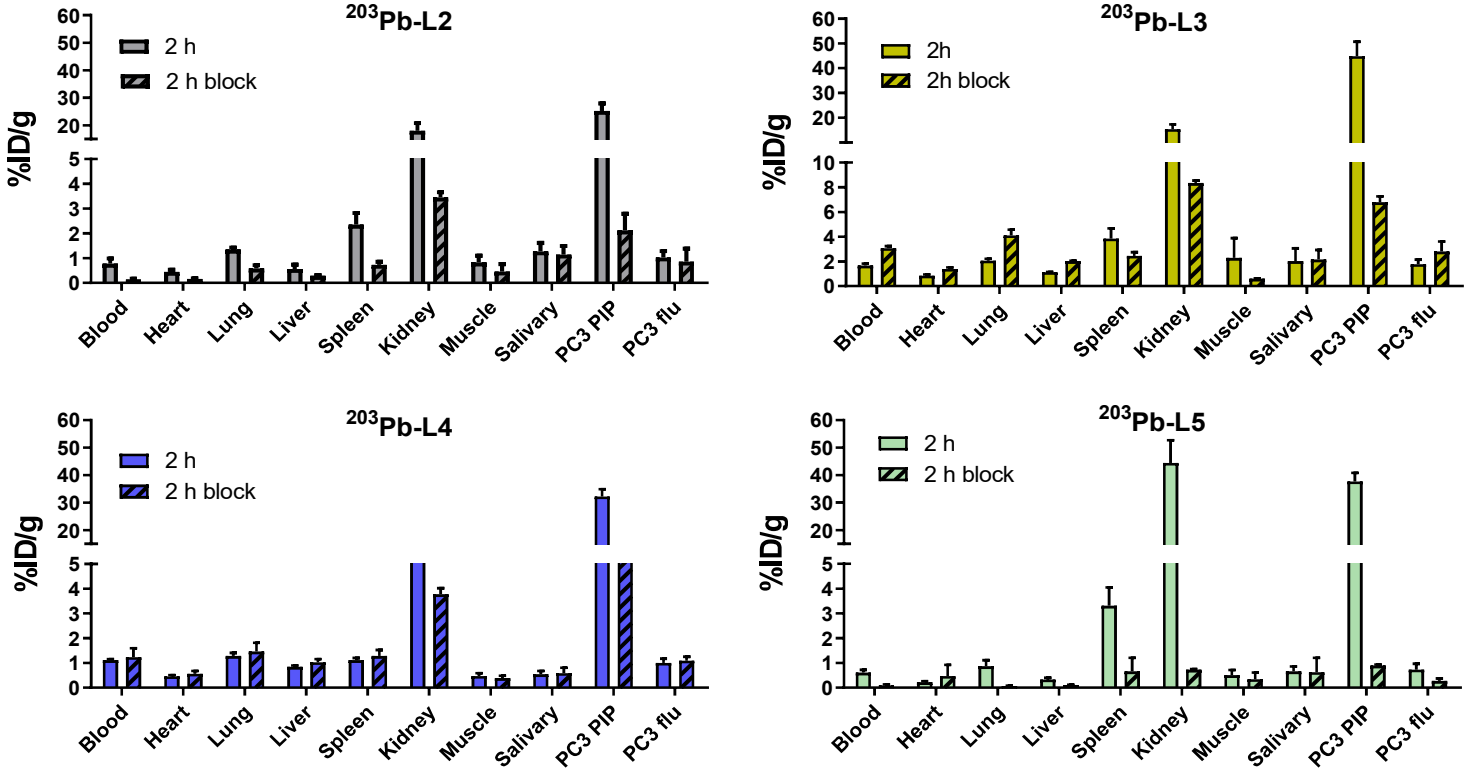

Comparison of time-dependent uptake of blood (A), kidney (B) and PSMA(+) tumor (C) of ^{203}Pb-L1-^{203}Pb-L5.

Supplemental Figure 3. High resolution electrospray ionization mass spectrometry HR-ESI-MS (A) and ^{1}H NMR (B) of L2 in DMSO at room temperature.

A

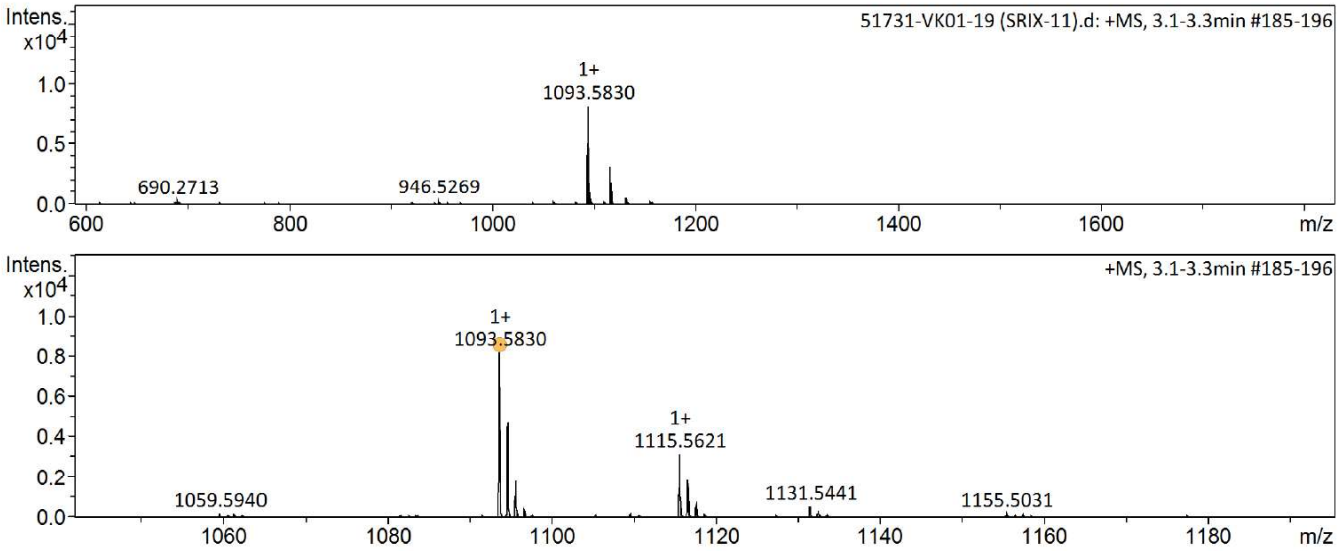

B

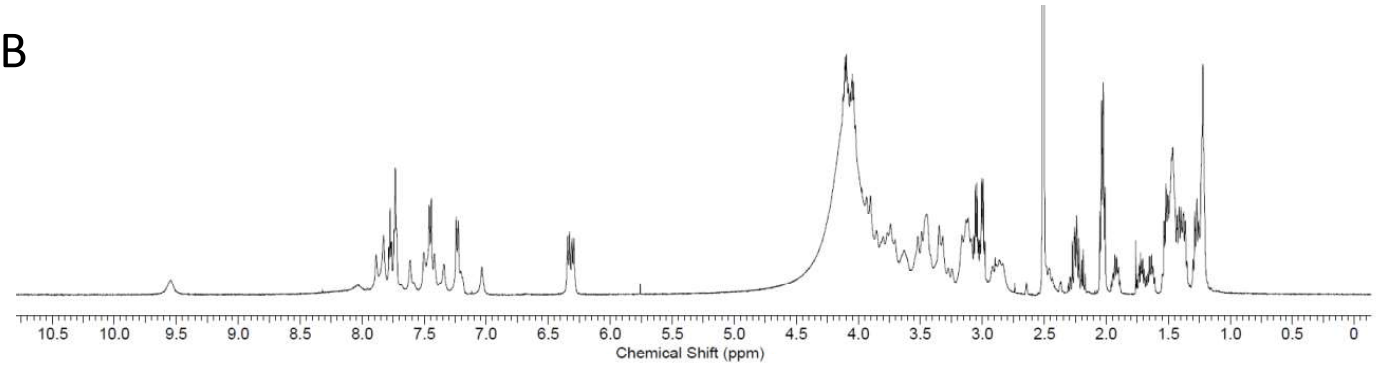

Supplemental Figure 4. High resolution electrospray ionization mass spectrometry (A) and ^{1}H NMR (B) of L3 in DMSO at room temperature.

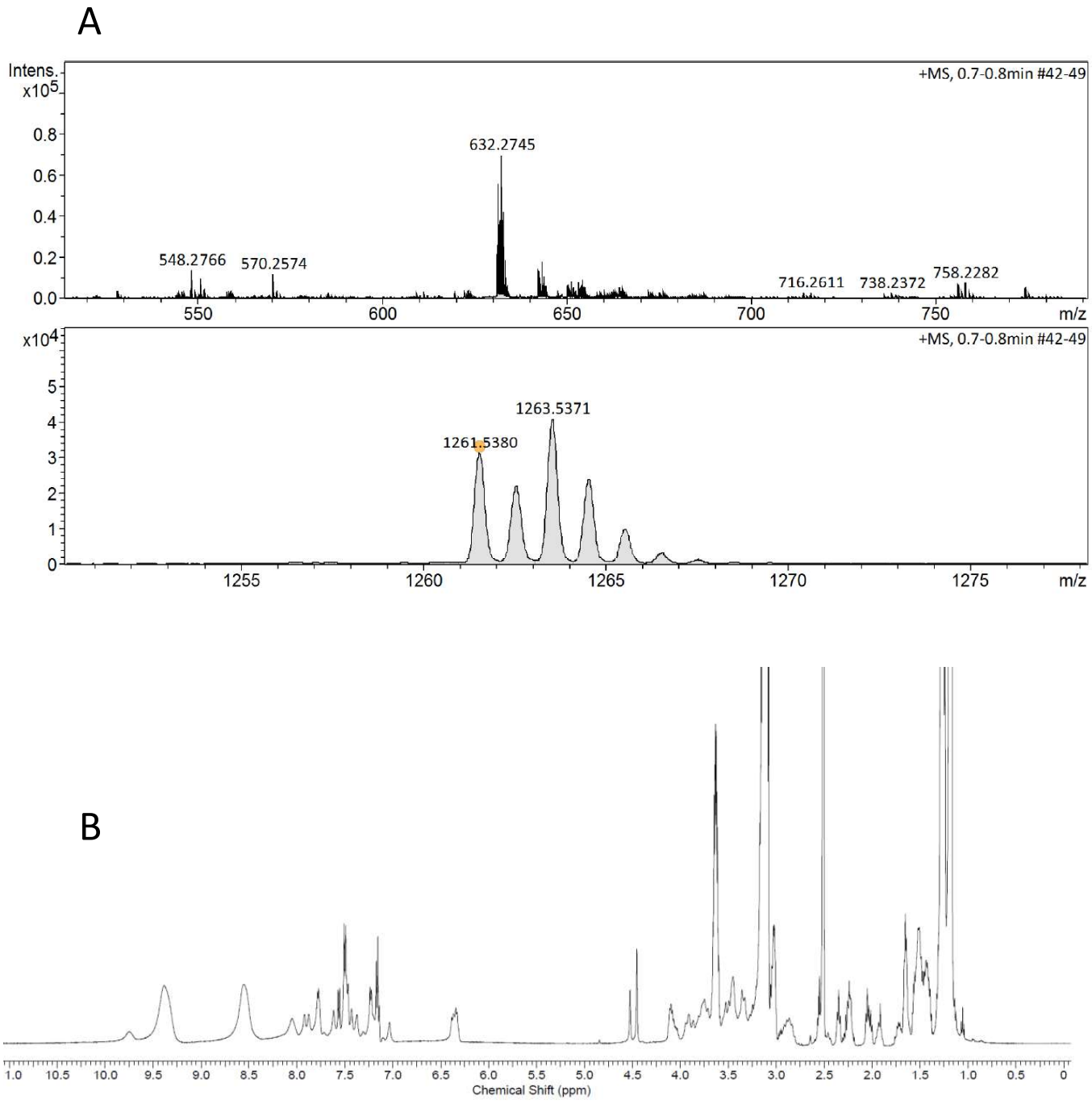

Supplemental Figure 5. High resolution electro-spray ionization mass spectrometry MS HR-ESI-MS (A) and ^{1}H NMR (B) of L4 in DMSO at room temperature.

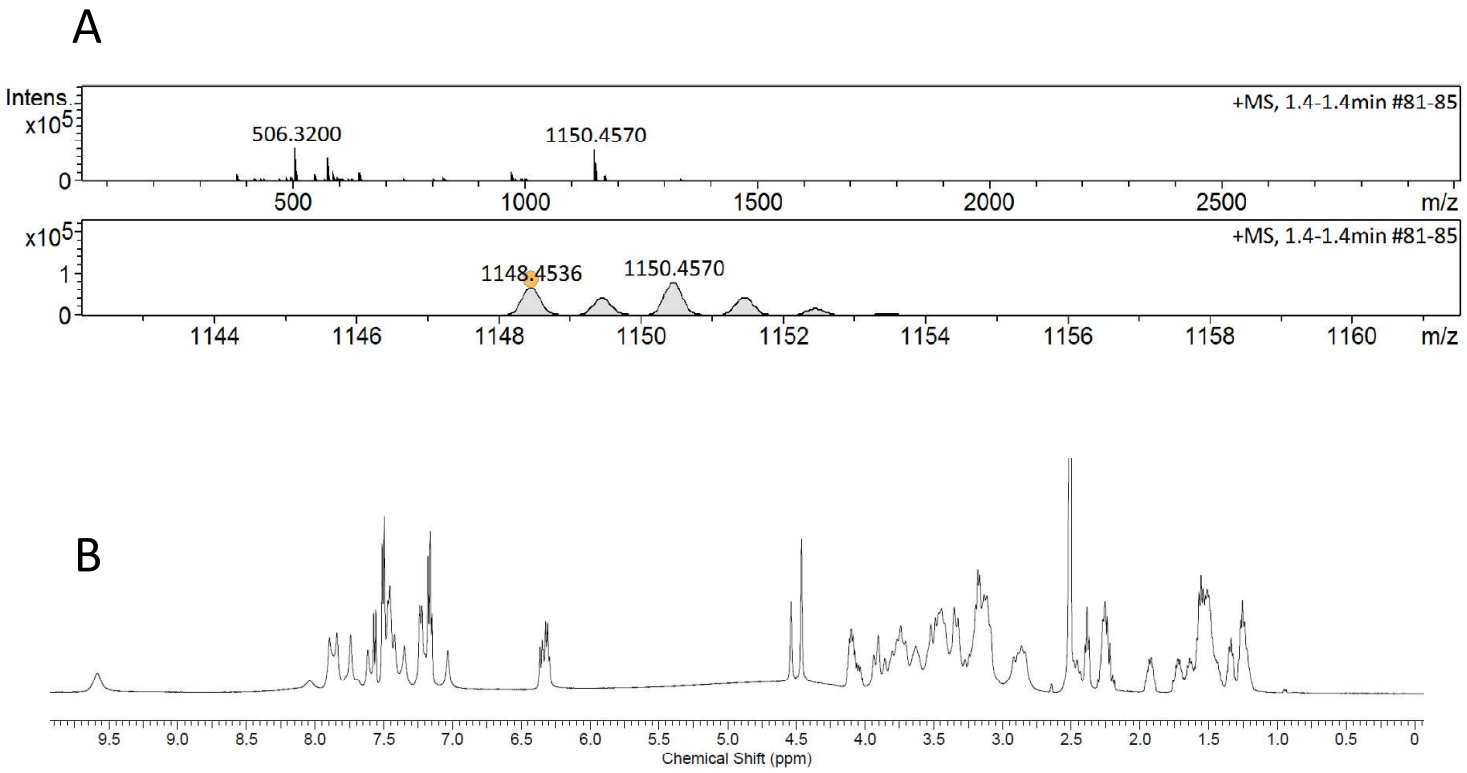

Supplemental Figure 6. High resolution electrospray ionization mass spectrometry MS HR-ESI-MS (A) and ^{1}H NMR (B) of L5 in DMSO at room temperature.

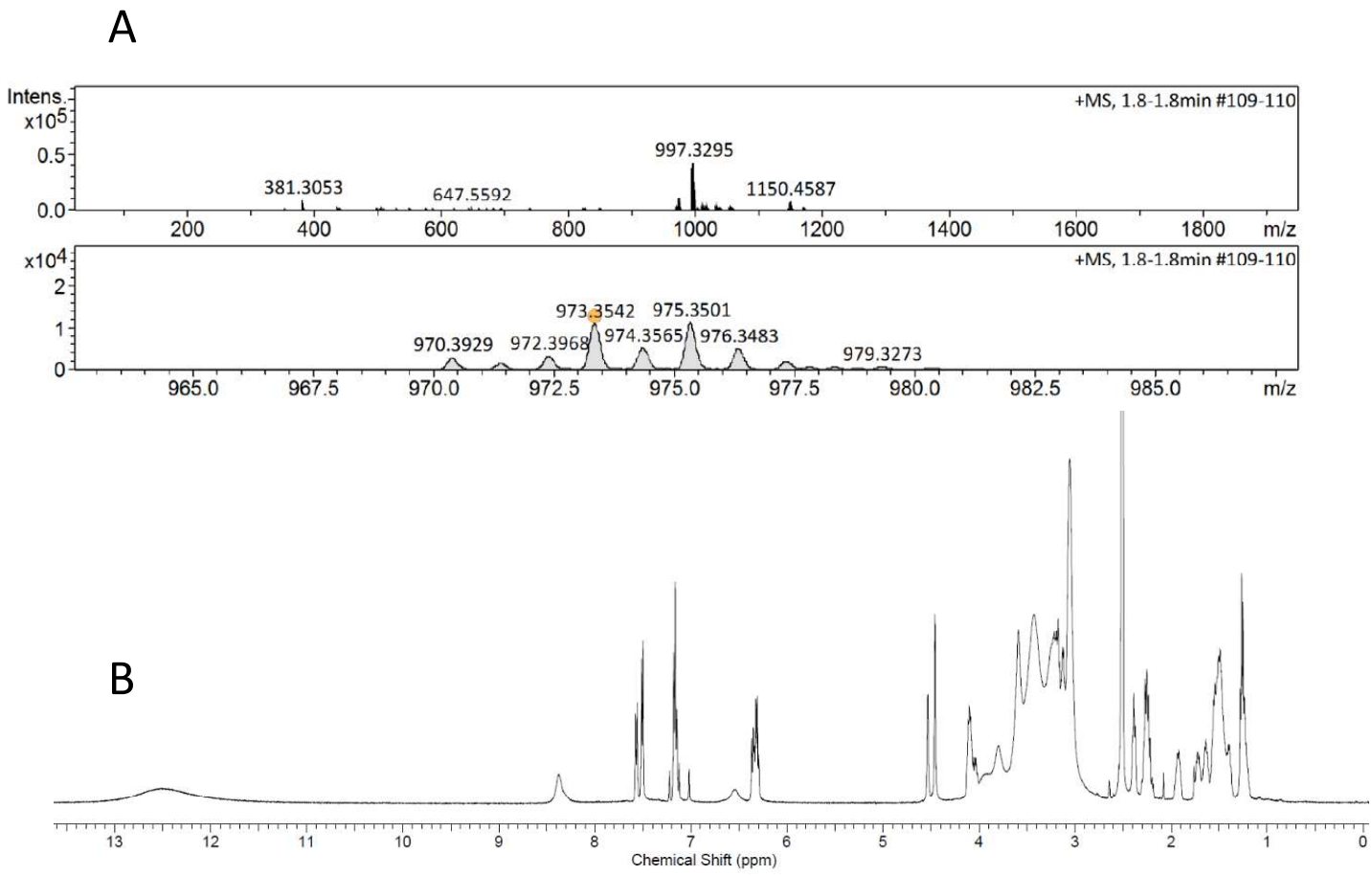

Supplemental Figure 7. HPLC chromatogram for ^{203}Pb-L1.
A. Radioactive peak at 24-25 min; B. UV peak (254 nm) associated with radioactive peak; C. UV peak (254 nm) at 22-24 min is for L1.

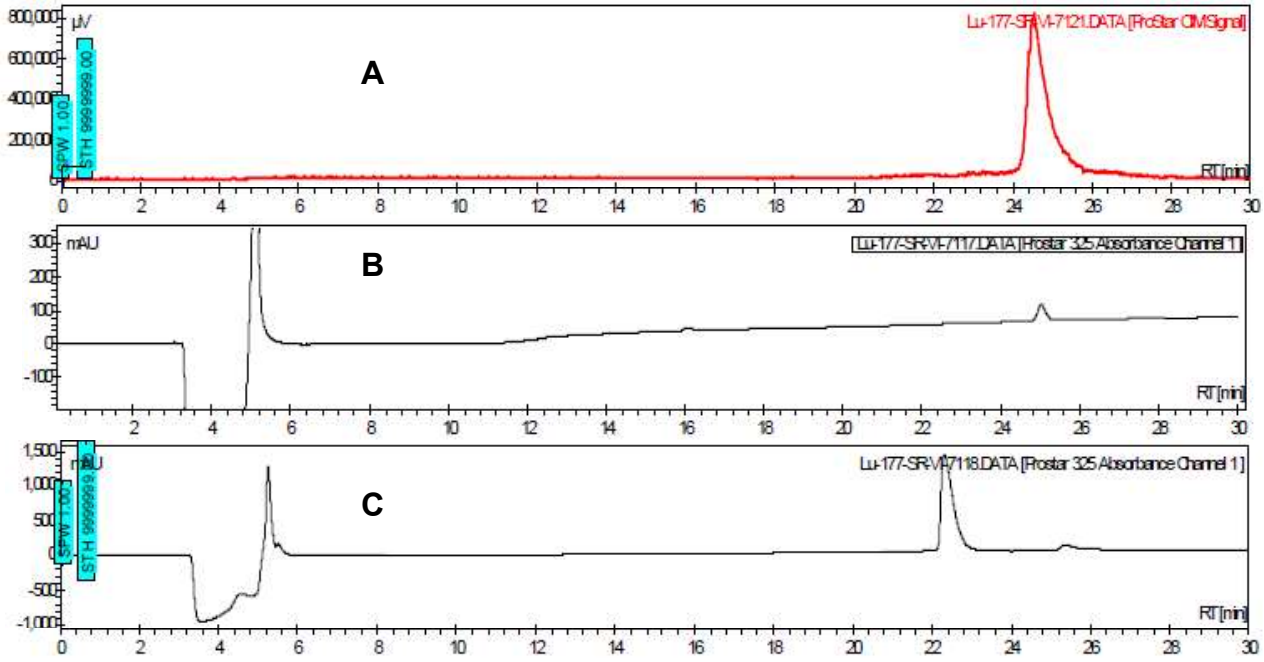

HPLC Method for ^{203}Pb-L1			
Min	Flow (mL/min)	Solvent A (10 mM ammonium acetate, pH 4.5)	Solvent B Acetonitrile
0	1	88	12
5	1	88	12
25	1	68	32
30	1	5	95
35	1	88	12

Supplemental Figure 8. HPLC chromatogram for ^{203}Pb-L2. A. Radioactive peak; B. UV peak (254 nm) at 16-17 min is associated with the radioactive peak and UV peak (254 nm) at 15.1-15.8 min is for unreacted L2.

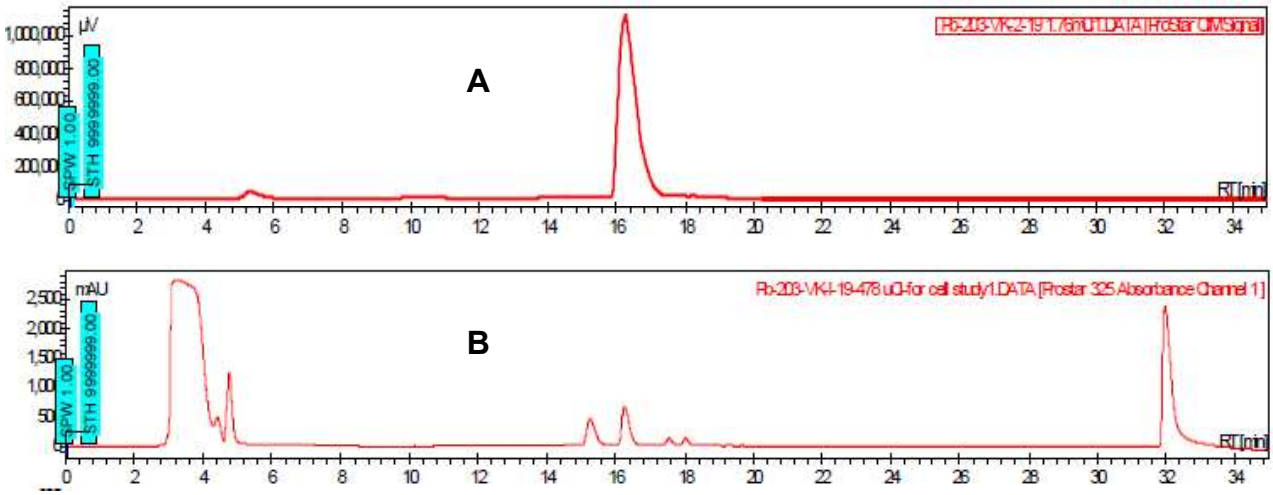

HPLC Method for ^{203}Pb-L2			
Min	Flow (mL/min)	Solvent A (10 mM ammonium acetate, pH 4.5)	Solvent B Acetonitrile
0	1	88	12
5	1	88	12
25	1	68	32
30	1	5	95
35	1	88	12

Supplemental Figure 9. HPLC chromatogram for ^{203}Pb-L3. A. Radioactive peak at 22-22 min; B. UV peak (254 nm) showing cold stable Pb-L2 peak

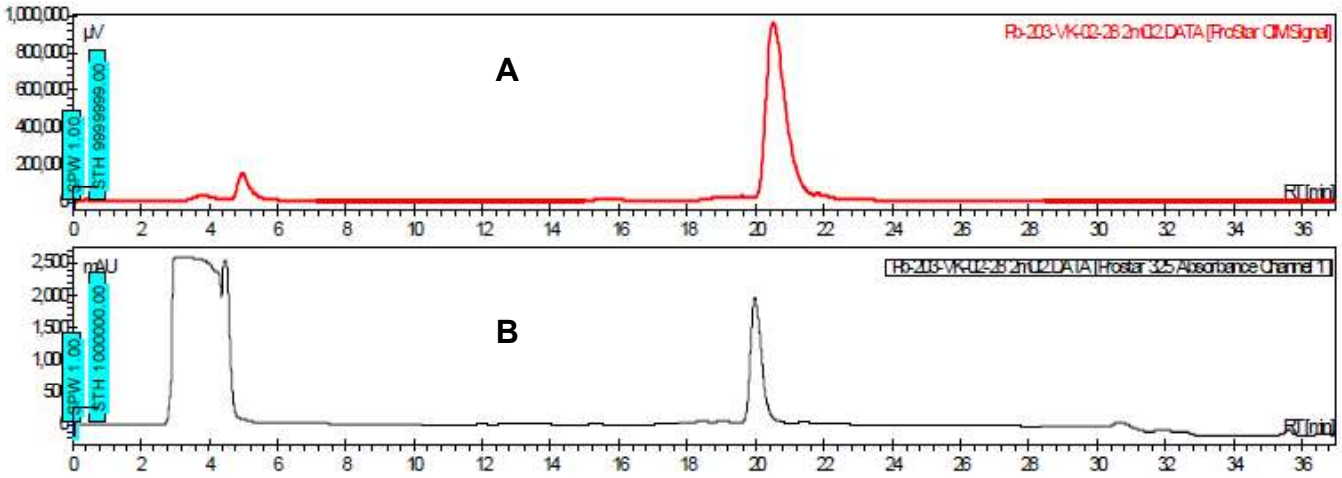

HPLC Method for ^{203}Pb-L3			
Min	Flow (mL/min)	Solvent A (10 mM ammonium acetate, pH 4.5)	Solvent B Acetonitrile
0	1	88	12
5	1	88	12
25	1	68	32
30	1	5	95
35	1	88	12

Supplemental Figure 10. HPLC chromatogram for ^{203}Pb-L4. A. Radioactive peak at 32-36 min; B. UV peak (254 nm) showing unreacted L4 at 30-32 min and UV-peak associated with the radiolabeled peak at 32-36 min; C. UV peak (254 nm) at 32-34 min for cold Pb-L4.

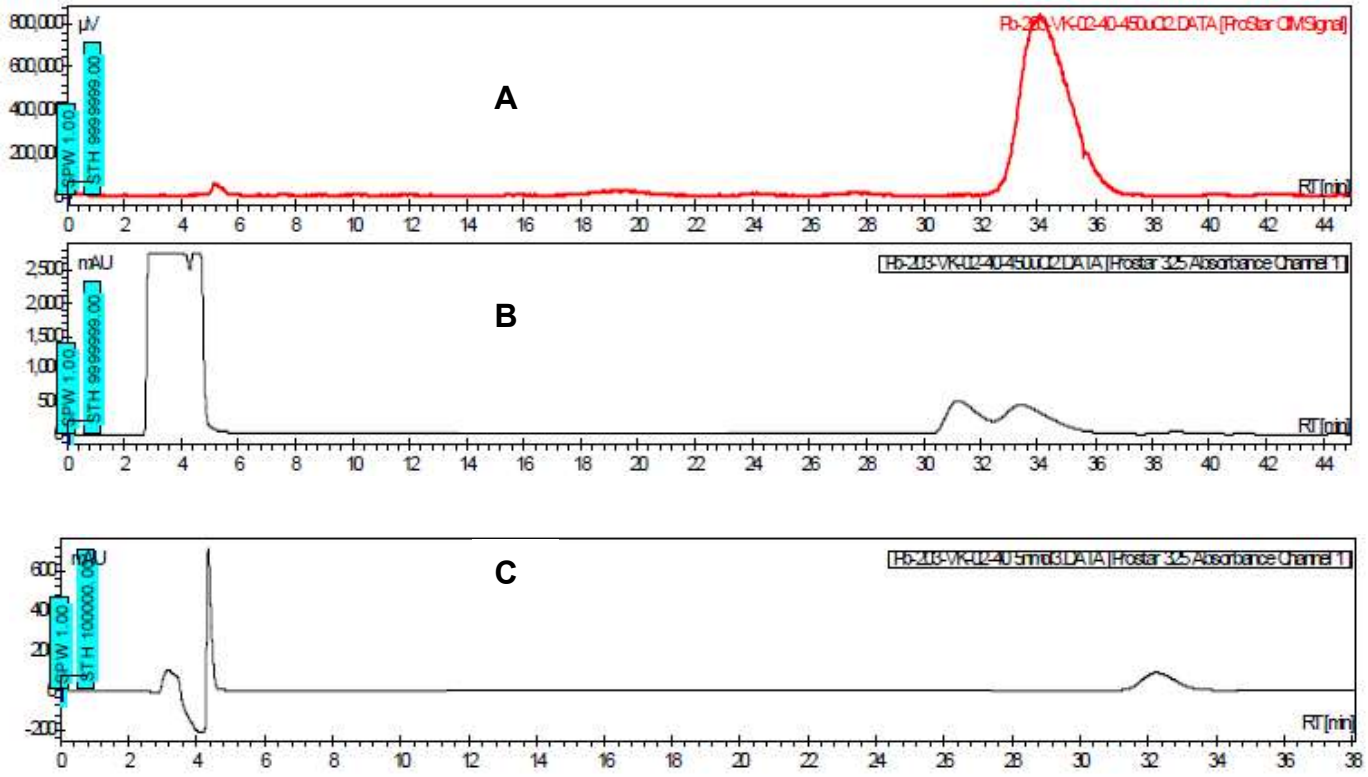

HPLC Method for ^{203}Pb-L4			
Min	Flow (mL/min)	Solvent A (10 mM ammonium acetate, pH 4.5)	Solvent B Acetonitrile
0	1	77	23
5	1	77	23
25	1	57	43
30	1	5	95
35	1	77	23

Supplemental Figure 11. HPLC chromatogram for ^{203}Pb-L5. A. Radioactive peak at 20-22 min; B. UV peak (254 nm) at 19.8-20.8 was associated with the radiolabeled peak; C. UV peak (254 nm) at 17.8-18.4 min was for L5.

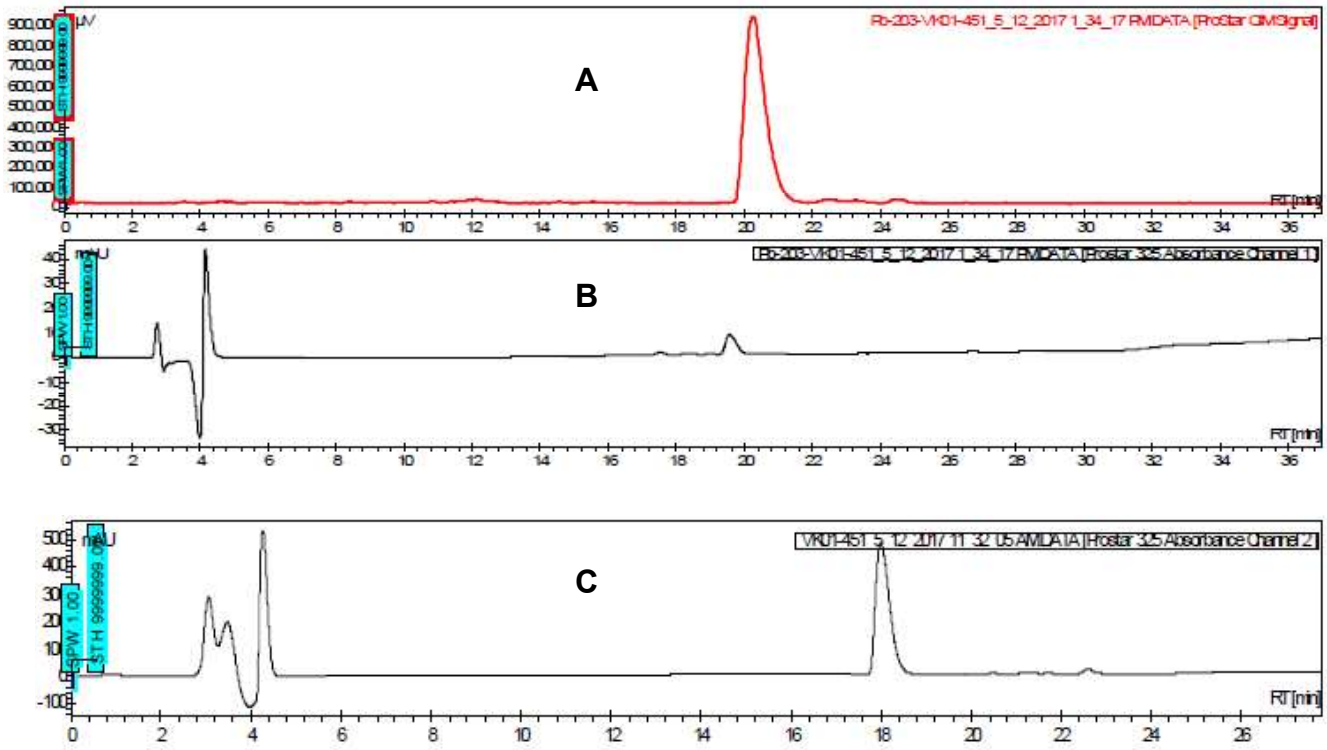

HPLC Method for ^{203}Pb-L5			
Min	Flow (mL/min)	Solvent A (10 mM ammonium acetate, pH 4.5)	Solvent B Acetonitrile
0	1	88	12
5	1	88	12
25	1	68	32
30	1	5	95
35	1	88	12

Supplemental Figure 12. HPLC chromatogram for ^{177}Lu-PSMA-617. A. Radioactive peak at 20-22 min; B. UV peak (254 nm) at 20-22 min associated with the radiolabeled peak and for peak at 29.8-30.8 min was related to the unlabeled PSMA-617.

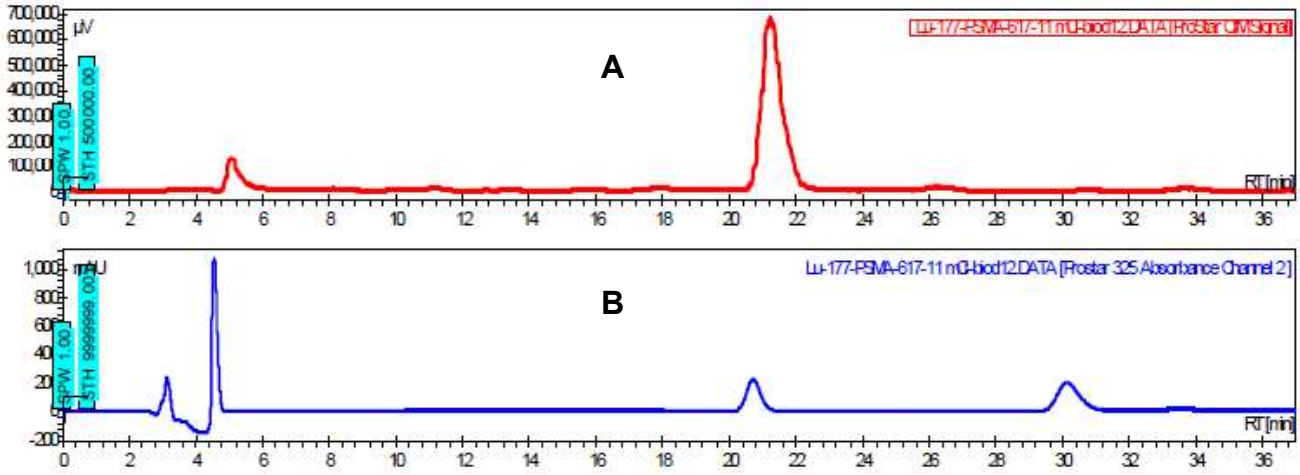

HPLC Method for ^{177}Lu-PSMA-617 (isocratic)			
Min	Flow (mL/min)	Solvent A (10 mM ammonium acetate, pH 4.5)	Solvent B Acetonitrile
0	1	78	22
5	1	78	22
45	1	78	22

SUPPLEMENTAL TABLE 1. Tissue biodistribution of ^{203}Pb-L1 in male NOD-SCID mice bearing PSMA(+) PC3 PIP and PSMA(-) PC3 flu tumors in either flank. Data are shown as %ID/g, expressed as mean ± SEM (n = 4)

Tissue	1 h	2 h	4 h	24 h
Blood	0.60±0.05	0.31±0.04	0.24±0.02	0.21±0.02
Heart	0.30±0.03	0.14±0.06	0.09±0.01	0.07±0.01
Lung	1.20±0.19	0.64±0.14	0.28±0.04	0.16±0.01
Liver	1.09±0.07	1.01±0.21	0.92±0.09	0.64±0.04
Stomach	0.30±0.04	0.15±0.03	0.13±0.03	0.07±0.01
Pancreas	0.49±0.09	0.29±0.05	0.24±0.05	0.09±0.06
Spleen	5.07±1.68	1.59±0.58	0.72±0.16	0.24±0.02
Fat	0.77±0.29	0.31±0.22	0.31±0.18	0.05±0.06
Kidney	75.2±9.94	39.4±7.28	22.8±6.22	7.01±0.80
Muscle	0.22±0.14	0.22±0.07	0.06±0.02	0.04±0.03
Small intestine	0.31±0.05	0.23±0.04	0.15±0.04	0.04±0.03
Salivary gland	1.78±0.69	0.93±0.07	0.29±0.02	0.10±0.05
Bladder	5.96±2.24	10.4±3.21	1.94±0.49	0.31±0.16
PSMA(+) PC3 PIP tumor	41.9±7.60	38.1±6.30	34.7±7.37	27.9±7.01
PSMA(-) PC3 flu tumor	0.43±0.11	0.29±0.14	0.20±0.06	0.14±0.01

SUPPLEMENTAL TABLE 2. Tissue biodistribution of ^{203}Pb-L2 in male NOD-SCID mice bearing PSMA(+) PC3 PIP and PSMA(-) PC3 flu tumors in either flank. Data are shown as %ID/g, expressed as mean ± SEM (n = 4).

Tissue	0.5 h	1 h	2 h	4 h	24 h	2 h Block
Blood	2.39 ± 0.33	0.77 ± 0.25	0.78 ± 0.42	0.04 ± 0.01	0.01 ± 0.00	0.14 ± 0.05
Heart	1.07 ± 0.16	0.43 ± 0.16	0.44 ± 0.17	0.06 ± 0.03	0.02 ± 0.00	0.15 ± 0.07
Lung	2.58 ± 0.67	1.23 ± 0.61	1.34 ± 0.17	0.19 ± 0.09	0.06 ± 0.01	0.58 ± 0.26
Liver	0.63 ± 0.04	0.42 ± 0.15	0.57 ± 0.34	0.17 ± 0.04	0.12 ± 0.01	0.29 ± 0.06
Stomach	1.00 ± 0.19	1.44 ± 1.65	1.48 ± 1.27	0.09 ± 0.04	0.05 ± 0.02	0.54 ± 0.50
Pancreas	0.54 ± 0.07	0.37 ± 0.23	0.60 ± 0.50	0.09 ± 0.06	0.02 ± 0.01	0.20 ± 0.09
Spleen	3.79 ± 0.86	1.88 ± 1.15	2.36 ± 0.94	0.34 ± 0.08	0.23 ± 0.04	0.73 ± 0.23
Fat	0.76 ± 0.14	1.62 ± 2.13	1.50 ± 1.44	0.09 ± 0.05	0.08 ± 0.02	0.10 ± 0.04
Kidney	33.81 ± 6.90	22.99 ± 11.92	18.05 ± 5.55	3.76 ± 1.03	3.11 ± 0.79	3.45 ± 0.41
Muscle	0.71 ± 0.32	1.07 ± 0.72	0.84 ± 0.51	0.08 ± 0.04	0.04 ± 0.034	0.46 ± 0.61
Sml intestine	0.98 ± 0.35	1.00 ± 1.09	1.03 ± 0.83	0.16 ± 0.18	0.04 ± 0.01	0.33 ± 0.12
Large intestine	1.70 ± 1.51	0.93 ± 0.56	4.02 ± 5.60	0.23 ± 0.15	0.07 ± 0.017	4.90 ± 8.07
Saliv glands	1.26 ± 0.17	5.29 ± 8.69	0.76 ± 0.23	0.12 ± 0.03	0.05 ± 0.01	0.28 ± 0.15
Bladder	38.22± 12.05	53.46 ± 35.17	15.88 ± 7.79	2.39 ± 2.55	0.52 ± 0.19	4.01 ± 2.74
PSMA(+) PC3 PIP tumor	18.55 ± 3.40	22.46 ± 8.12	25.24 ± 5.35	11.63 ± 4.19	8.54 ± 2.06	2.12 ± 1.33
PSMA(-) PC3 flu tumor	1.26 ± 0.20	1.49 ± 1.19	1.03 ± 0.51	0.14 ± 0.04	0.08 ± 0.02	0.86 ± 1.06

SUPPLEMENTAL TABLE 3. Tissue biodistribution of ^{203}**Pb-L3** in male NOD-SCID mice bearing PSMA(+) PC3 PIP and PSMA(-) PC3 flu tumors in either flank. Data are shown as %ID/g, expressed as mean ± SEM (n = 4).

Tissue	0.5 h	1 h	2 h	4 h	24 h	2h Block
Blood	9.43 ± 0.86	4.42 ± 0.69	1.66 ± 0.36	0.33 ± 0.10	0.05 ± 0.00	3.07 ± 0.35
Heart	5.07 ± 4.04	1.70 ± 0.13	0.86 ± 0.15	0.20 ± 0.03	0.12 ±0.01	1.40 ± 0.24
Lung	5.76 ± 3.04	4.13 ± 1.20	2.07 ± 0.31	0.72 ± 0.23	0.25 ± 0.08	4.10 ± 0.94
Liver	2.19 ± 0.45	1.57 ± 0.18	1.13 ± 0.07	0.69 ± 0.10	0.93 ± 0.19	2.03 ± 0.05
Stomach	3.24 ± 1.59	2.09 ± 1.54	1.63 ± 1.88	0.34 ± 0.23	0.77 ± 0.86	0.85 ± 0.05
Pancreas	2.54 ± 1.94	0.85 ± 0.15	0.64 ± 0.18	0.19 ± 0.09	0.10 ± 0.02	1.00 ± 0.54
Spleen	5.73 ± 2.60	4.60 ± 1.70	3.86 ± 1.65	1.15 ± 0.30	0.86 ± 0.50	2.46 ± 0.58
Fat	1.27 ± 0.72	1.12 ± 0.40	1.50 ± 1.16	0.19 ± 0.08	0.28 ± 0.14	0.83 ± 0.245
Kidney	56.73 ± 21.55	22.16 ± 14.46	15.41 ± 3.78	6.44 ± 1.76	4.61 ± 0.47	8.35 ± 0.39
Muscle	1.27 ± 0.47	1.23 ± 0.56	2.29 ± 3.19	0.13 ± 0.02	0.14 ± 0.09	0.61 ± 0.07
Small intestine	1.81 ± 0.25	1.50 ± 0.78	0.77 ± 0.35	0.42 ± 0.29	0.36 ± 0.32	1.00 ± 0.21
Large intestine	4.40 ± 2.88	1.14 ± 0.65	2.03 ± 2.04	0.55 ± 0.46	0.40 ± 0.50	2.16 ± 1.55
Salivary glands	4.38 ± 2.82	1.77 ± 0.16	0.94 ± 0.12	0.29 ± 0.04	0.22 ± 0.06	1.63 ± 0.51
Bladder	28.82 ± 18.62	24.86 ± 30.96	13.13 ± 1.59	3.38 ± 1.92	0.75 ± 0.17	23.51 ± 7.72
PSMA(+) PC3 PIP tumor	28.25 ± 6.16	37.48 ± 8.98	44.92 ± 11.71	24.87 ± 7.44	24.17 ± 9.30	6.79 ± 0.94
PSMA(-) PC3 flu tumor	2.44 ± 0.50	1.35 ± 0.91	1.77 ± 0.78	0.45 ± 0.07	0.26 ± 0.03	2.80 ± 1.63

SUPPLEMENTAL TABLE 4. Tissue biodistribution of ^{203}Pb-L4 in male NOD-SCID mice bearing PSMA(+) PC3 PIP and PSMA(-) PC3 flu tumors in either flank. Data are shown as %ID/g, expressed as mean ± SEM (n = 4).

	0.5h	1h	2h	4h	24h	2h Block
Blood	7.09 ± 0.90	3.96 ± 0.78	1.16 ± 0.08	0.31 ± 0.12	0.07 ± 0.07	1.24 ± 0.72
Heart	2.80 ± 0.66	1.40 ± 0.33	0.47 ± 0.08	0.17 ± 0.05	0.08 ± 0.02	0.56 ± 0.24
Lung	5.15 ± 0.50	3.15 ± 0.44	1.28 ± 0.25	0.54 ± 0.16	0.30 ± 0.27	1.46 ± 0.71
Liver	1.82 ± 0.15	1.24 ± 0.20	0.84 ± 0.10	0.57 ± 0.08	0.59 ± 0.11	1.03 ± 0.24
Stomach	1.57 ± 0.21	1.64 ± 1.24	2.58 ± 3.37	0.37 ± 0.26	0.09 ± 0.02	0.44 ± 0.12
Pancreas	1.02 ± 0.13	0.71 ± 0.24	0.35 ± 0.18	0.10 ± 0.03	0.05 ± 0.02	0.34 ± 0.16
Spleen	4.89 ± 0.38	2.85 ± 0.76	1.11 ± 0.18	0.67 ± 0.23	0.50 ± 0.18	1.29 ± 0.49
Fat	2.27 ± 0.72	3.47 ± 4.14	1.50 ± 1.92	0.25 ± 0.22	0.15 ± 0.07	0.63 ± 0.24
Kidney	35.87 ± 8.51	20.31 ± 2.96	10.29 ± 2.10	6.02 ± 1.45	2.61 ± 0.47	3.78 ± 0.49
Muscle	1.09 ± 0.33	0.99 ± 0.56	0.47 ± 0.23	0.26 ± 0.22	0.19 ± 0.21	2.39 ± 4.18
Sm Intestine	1.33 ± 0.23	0.95 ± 0.60	1.93 ± 3.19	0.12 ± 0.06	0.09 ± 0.02	0.73 ± 0.40
Lrg Intestine	1.44 ± 0.35	2.67 ± 3.29	0.55 ± 0.27	0.45 ± 0.31	0.09 ± 0.02	2.59 ± 3.87
Sal Glnds	2.17 ± 0.25	1.32 ± 0.42	0.43 ± 0.06	0.28 ± 0.18	0.11 ± 0.02	1.16 ± 1.40
Bladder	18.79 ± 6.37	52.30 ± 36.76	33.61 ± 33.85	7.82 ± 5.31	0.37 ± 0.22	30.85 ± 31.13
PSMA(+) PC3 PIP tumor	27.27 ± 3.43	31.10 ± 8.26	32.19 ± 5.42	27.66 ± 9.38	16.44 ± 8.72	6.22 ± 1.70
PSMA(-) PC3 flu tumor	2.13 ± 0.40	2.06 ± 0.48	1.00 ± 0.34	0.61 ± 0.41	0.21 ± 0.06	1.10 ± 0.32

SUPPLEMENTAL TABLE 5. Tissue biodistribution of ^{203}Pb-L5 in male NOD-SCID mice bearing PSMA(+) PC3 PIP and PSMA(-) PC3 flu tumors in either flank. Data are shown as %ID/g, expressed as mean ± SEM (n = 4).

	30 min	1 h	2 h	2 h blocking	4 h	24 h
Blood	1.76 ± 0.16	0.67 ± 0.21	0.47 ± 0.31	1.34 ± 2.59	2.02 ± 3.12	0.02 ± 0.01
Heart	0.72 ± 0.13	0.30 ± 0.10	0.22 ± 0.10	0.48 ± 0.89	0.81 ± 1.23	0.02 ± 0.02
Lung	2.42 ± 0.47	1.30 ± 0.46	0.87± 0.50	1.37 ± 2.58	2.64 ± 3.84	0.07 ± 0.06
Liver	0.89 ± 0.10	0.43 ± 0.13	0.33 ± 0.14	0.69 ± 1.17	1.09 ± 1.53	0.07 ± 0.05
Stomach	0.92 ± 0.18	0.44 ± 0.23	0.33 ± 0.11	0.59 ± 0.97	1.09 ± 1.61	0.03 ± 0.02
Pancreas	1.01 ± 0.50	0.52 ± 0.13	0.53 ± 0.16	0.45 ± 0.69	0.76± 0.97	0.01 ± 0.01
Spleen	7.54 ± 1.81	5.97 ± 2.18	3.31 ± 1.48	0.66 ± 1.09	3.77 ± 3.41	0.17 ± 0.21
Fat	0.55 ± 0.04	0.47 ± 0.14	0.47 ± 0.42	0.25 ± 0.35	0.47 ± 0.58	0.01 ± 0.01
Kidney	82.23 ± 13.53	63.78 ± 7.36	44.46 ± 16.38	5.46 ± 9.47	38.90 ± 18.03	5.30 ± 5.34
Muscle	0.50 ± 0.08	0.29 ± 0.10	0.51 ± 0.42	0.35 ± 0.53	0.47 ± 0.67	0.01 ± 0.00
Small Intestine	0.74 ± 0.09	0.43 ± 0.16	0.48 ± 0.31	0.86 ± 1.57	1.16 ± 1.75	0.03 ± 0.02
Salivary Glands	1.29 ± 0.21	0.78 ± 0.30	0.66 ± 0.40	0.63 ± 1.17	1.29 ± 1.76	0.03 ± 0.03
Lacrimal Gland	2.33 ± 0.89	1.87± 0.67	0.61 ± 0.29	0.72 ± 1.03	1.35 ± 1.77	0.06 ± 0.03
Bladder	23.92 ± 11.98	30.69 ± 21.82	23.54 ± 6.77	24.72 ± 24.95	18.03 ± 12.10	0.26 ± 0.08
Bone	0.97 ± 0.51	0.38 ± 0.18	2.50 ± 3.65	0.73 ± 0.82	1.47 ± 1.13	0.04 ± 0.01
PSMA(+) PC3 PIP tumor	36.53 ± 1.93	45.37 ± 9.30	37.67 ± 6.26	1.80 ± 1.82	55.81 ± 22.42	42.61 ± 12.97
PSMA(-) PC3 flu tumor	1.94 ± 1.31	0.91 ± 0.35	0.74 ± 0.46	1.11 ± 1.68	1.86 ± 2.56	0.05 ±0.03

SUPPLEMENTAL TABLE 6. Murine organ absorbed dose coefficients of ^{212}Pb-L1-^{212}Pb-L5 determined from the corresponding murine biodistribution data. Only α-particle deposition was considered.

Tissue	^{203}Pb-L1	^{203}Pb-L2	^{203}Pb-L3	^{203}Pb-L4	^{203}Pb-L5
	(mGy/kBq)	*(mGy/kBq)*	*(mGy/kBq)*	*(mGy/kBq)*	*(mGy/kBq)*
Blood	0.167	0.135	0.528	0.435	0.389
Heart	0.063	0.081	0.297	0.194	0.178
Lung	0.205	0.234	0.615	0.504	0.610
Liver	0.526	0.138	0.663	0.457	0.278
Stomach	0.072	0.190	0.727	0.348	0.243
Pancreas	0.129	0.086	0.193	0.105	0.192
Spleen	0.540	0.431	1.040	0.575	1.273
Fat	0.144	0.203	0.300	0.351	0.140
Kidneys	12.711	4.409	5.800	4.193	15.180
Muscle	0.074	0.130	0.279	0.202	0.127
Small intestine	0.033	0.158	0.347	0.230	0.262
Large intestine	N/A	0.375	0.507	0.271	N/A
Salivary glands	0.241	0.281	0.347	0.211	0.316
Urinary bladder	1.448	4.128	3.143	5.571	5.766
PSMA(+) PC3 PIP tumor	23.111	8.014	18.269	14.958	30.997
PSMA(+) PC3 flu tumor	0.126	0.191	0.385	0.370	0.443
Bone	N/A	N/A	N/A	N/A	0.442
Lacrimal gland	N/A	N/A	N/A	N/A	0.407

SUPPLEMENTAL TABLE 7. Selected Human organ absorbed dose coefficients of ^{212}Pb-L1-^{212}Pb-L5 estimated based on the murine biodistribution data using OLINDA/EXM version 1 (*1*).

	Absorbed Dose Coefficient (mGy/MBq)			
^{212}Pb-L1	Alpha	Beta	Photon	Total
Kidneys	4.31	0.48	0.05	4.84
Spleen	0.18	0.02	0.01	0.21
Liver	0.18	0.02	0.01	0.21
Salivary glands (44.5 g)	N/A	N/A	N/A	0.09
PIP-Tumor (1 gram)	N/A	N/A	N/A	9.36
^{212}Pb-L2	Alpha	Beta	Photon	Total
Kidneys	1.50	0.17	0.02	1.69
Spleen	0.15	0.02	0.01	0.17
Liver	0.05	0.01	0.00	0.06
Salivary glands (44.5 g)	N/A	N/A	N/A	0.11
PIP-Tumor (1 gram)	N/A	N/A	N/A	2.99
^{212}Pb-L3	Alpha	Beta	Photon	Total
Kidneys	1.97	0.22	0.03	2.22
Spleen	0.35	0.04	0.01	0.40
Liver	0.23	0.03	0.01	0.26
Salivary glands (44.5 g)	N/A	N/A	N/A	0.13
PIP-Tumor (1 gram)	N/A	N/A	N/A	6.81
^{212}Pb-L4	Alpha	Beta	Photon	Total
Kidneys	1.42	0.16	0.02	1.60
Spleen	0.20	0.02	0.01	0.22
Liver	0.16	0.02	0.01	0.18
Salivary glands (44.5 g)	N/A	N/A	N/A	0.08
PIP-Tumor (1 gram)	N/A	N/A	N/A	5.58
^{212}Pb-L5	Alpha	Beta	Photon	Total
Kidneys	5.15	0.58	0.06	5.79
Spleen	0.43	0.05	0.01	0.49
Liver	0.09	0.01	0.01	0.11
Salivary glands (44.5 g)	N/A	N/A	N/A	0.12
PIP-Tumor (1 gram)	N/A	N/A	N/A	11.60

SUPPLEMENTAL TABLE 8. Blood chemistry in CD-1 mice (n = 7) at 7 months after single administration of 3.7 MBq ^{212}Pb-L2.

	Mouse number	Complete Blood Counts	Creatinine	Alanine Aminotransferase (U/L)	Aspartate Aminotransferase (U/dL)	Blood urea nitrogen (mg/dL)
^{212}Pb-L2			(0.2-0.9)	(26-77)	(54-269)	(8-33)
3.7 MBq	1	Died				
	2	Normal	1.4	47	112	258
	3	Normal	0.8	20	43	67
	4	Normal	0.6	78	96	49
	5	Died				
	6	Normal	1.8	24	41	196
	7	Normal	1.3	63	86	68
Control	15	Normal	0.4	90	125	25

SUPPLEMENTAL TABLE 9. Selected chemistry panel (metabolic profile) and lipid profile of the mice administered with a single dose of ^{212}Pb-L2 and control (saline treatment) at one-year post-treatment (n = 3).

	Control	Control	Control	0.74 MBq	0.74 MBq	0.74 MBq	0.74 MBq	1.5 MBq	1.5 MBq
Body Weight	55.0	54.8	45.6	47.9	59.4	53.2	50.3	49.4	54.7
Chemistry									
Na	156	157	150	163	163	150	149	154	161
Cl	119	118	113	127	126	116	110	118	125
K	13.6	11.6	11.3	10	11.5	11.9	10.5	8.7	10.9
Blood urea nitrogen (mg/dL)	19	23	18	14	16	18	11	24	44
Creatinine (mg/dL)	0.3	0.2	0.3	0.1	0.2	0.2	0.3	0.2	0.3
Aspartate Aminotransferase (U/L)	247	123	73	116	86	85	82	84	75
Alanine Aminotransferase (U/dL)	72	94	42	79	48	51	23	37	30
Cholesterol (mg/dL)	236	137	210	154	237	214	158	149	170
Triglycerides (mg/dL)	233	109	182	91	177	129	132	95	166
High-density lipoprotein (mg/dL)	114	72	111	86	105	117	86	80	85
Total protein (g/dL)	6.6	6.4	6	NA	5.4	NA	5.6	6.3	6.2
Albumin g/dL	3.2	3	2.6	3.1	2.7	NA	2.7	3	3
Total Bilirubin (mg/dL)	0.3	0.1	0.2	0.1	0.2	NA	0.2	0.2	0.3

SUPPLEMENTAL TABLE 10. Complete blood counts of the mice (n = 3) administered with a single dose of ^{212}Pb-L2 and control (saline treatment) at one-year post-treatment.

	control	control	control	^{212}Pb-L2 (0.74 MBq)	^{212}Pb-L2 (0.74 MBq)	^{212}Pb-L2 (0.74 MBq)	^{212}Pb-L2 (0.74 MBq)	^{212}Pb-L2 (1.5 MBq)	^{212}Pb-L2 (1.5 MBq)
Red blood cells (M/µL)	10.97	9.35	11.6	5.06	6.37	9.19	8.82	7.84	6.28
Hemoglobin (g/dL)	16.3	13.2	17.9	8	9.9	13.9	13	10.8	8.7
Hematocrit %	54.8	42.4	61.5	26.4	31.8	45.9	42.2	35.6	26.4
Platelets (K/µL)	1845	2784	1453	1228	1415	1456	1431	1282	1732
White blood cells (K/µL)	5.51	8.76	27.33	41.8	8.7	9.39	12.52	16.27	10.11
Neutrophils (K/µL)	3.94	6.3	10.45	9.66	4.75	4.06	7.06	7.31	5.55
Lymphocytes (K/µL)	1.36	2.01	15.66	17.54	3.62	5	4.78	7.94	3.83
Monocytes (K/µL))	0.21	0.44	0.85	14.59	0.31	0.27	0.5	0.93	0.66
Reticulocytes (K/µL)	571.5	373.1	641.5	181.1	250.3	405.3	508.9	327.7	304.6
Urine									
Sp. gravity	1.051	1.035	1.035	>1.060	>1.060	1.047	1.032	1.047	1.044
Protein	2	1.6	1.8	2.1	2.7	1.8	1.7	1.6	1.4

SUPLEMENTARY TABLE 11. Selected perfused organ weight of the mice (n = 3) administered with a single dose of ^{212}Pb-L2 after 13 months post-administration.

	control	control	control	^{212}Pb-L2 (0.74 MBq)	^{212}Pb-L2 (0.74 MBq)	^{212}Pb-L2 (0.74 MBq)	^{212}Pb-L2 (0.74 MBq)	^{212}Pb-L2 (1.5 MBq)	^{212}Pb-L2 (1.5 MBq)
Body Weight	55.012	54.763	45.638	47.908	59.358	53.238	50.26	49.419	54.697
Organ Weights(g) perfused									
Liver g	2.689	2.811	2.881	3.272	3.383	3.016	2.27	2.053	2.446
Liver %	4.89	5.13	6.31	6.83	5.70	5.67	4.52	4.15	4.47
Spleen g	0.137	0.115	0.244	0.494	0.148	0.157	0.162	0.18	0.172
Spleen %	0.25	0.21	0.53	1.03	0.25	0.29	0.32	0.36	0.31
Heart	0.381	0.38	0.566	0.397	0.399	0.351	0.43	0.388	0.283
Right Kidney	0.516	0.526	0.486	0.567	0.668	0.547	0.49	0.413	0.573
Left Kidney	0.501	0.502	0.448	0.576	0.694	0.517	0.459	0.416	0.361

SUPPLEMENTAL EXPERIMENTAL METHODS

Chemistry

Ligand L1 (*2*) and L5 (*3*) and intermediates 3 (*4*) and 4 (*3*) were synthesized following our previous reports.

(15S,19S)-6,9,17-Trioxo-1-((4-((1,4,7,10-tetrakis(2-amino-2-oxoethyl)-1,4,7,10-tetraazacyclododecan-2-yl)methyl)phenyl)amino)-1-thioxo-2,5,10,16,18-pentaazahenicosane-15,19,21-tricarboxylic acid (L2). Ligand **L2** was synthesized following the scheme described in Supplemental Figure 1A, as following a method previously reported by us (*2*). Briefly, commercially available N-Boc-1,4-diaminobutane (81.4 mg, 0.43 mmol in 0.5 mL DMSO) was mixed with S-2-(4-Isothiocyanatobenzyl)-1,4,7,10-tetraaza-1,4,7,10-tetra(2-carbamoylmethyl)cyclododecane] (*p*-SCN-Bn-TCMC) (300 mg, 0.43 mmol in 1.5 mL DMSO) and DIEA (376 µL, 2.16 mmol) and stirred at 40°C for 4 h. The solvent was evaporated, and the residue was purified by reverse phase C_{18} flash chromatography (5.5 g, Agilent SF10) using water and acetonitrile (80/20, respectively, and with 0.1% TFA in each solvent). The pulled fractions containing compound **1** were lyophilized. ^{1}H NMR (DMSO-d_6) δ: 9.61 (bs, 1H), 8.06-6.82 (m, 13H), 4.00-3.14 (m, 24H, merged with water peak), 2.93-2.74 (m, 6H), 1.56-1.38 (13H). ESI-MS 736.42 $[M+H]^+$. Compound **1** was then treated with ice-cold TFA/CH_2Cl_2 (50/50) solution and left stirring at ambient temperature for 2 h. After solvent removal, the residue was dried under vacuum and purified by C_{18} flash chromatography (90/10 water/acetonitrile) to obtain compound **2** in moderate yield. ESI-MS: 636.36 $[M+1]^+$. To a solution of compound **2** (200 mg, 0.31 mmol in 1 mL DMSO) was added **3** (*4*) (198 mg, 0.34 mmol in 1 mL DMSO) and TEA (318 mg, 3.15 mmol), which was left stirring at ambient temperature for 2 h. After evaporation of solvent, the residue was dissolved in water and purified by HPLC to obtain **L2**. Elemental Anal. ($C_{48}H_{80}N_{14}O_{13}S$, $3.5CF_3COOH \cdot H_2O$) C, H, N, calculated: 43.74%, H 5.71%, N 12.98% S 2.12%; Found C 43.79%, H 5.64%, N 12.73% S1.90%.

(21S,25S)-16-(4-Bromobenzyl)-8,15,23-trioxo-1-((4-((1,4,7,10-tetrakis(2-amino-2-oxoethyl)-1,4,7,10-tetraazacyclododecan-2-yl)methyl)phenyl)amino)-1-thioxo-2,7,16,22,24-pentaazaheptacosane-21,25,27-tricarboxylic acid. (L3). L3 was synthesized following the same method as L2 by using the using the intermediate compound 4 as shown in Supplemental Fig. 1C.

Di-tert-butyl (((S)-6-(N-(4-bromobenzyl)-8-((2,5-dioxopyrrolidin-1-yl)oxy)-8-oxooctanamido)-1-(tert-butoxy)-1-oxohexan-2-yl)carbamoyl)-L-glutamate (Compound 4). Compound **5**, urea-lysine intermediate di-tert-butyl-(((S)-1-(tert-butoxy)-6-((4-bromobenzyl)amino)-1-oxohexan-2-yl)carbamoyl)-L-glutamate was synthesized following a literature method after minor modification (*5*). Compound 4 was synthesized following a route as shown in Fig. 1C. A solution of 5 (0.190 g, 0.29 mmol), Et_3N (0.029 g, 0.29 mmol) and DMF (1 mL) was added dropwise to a stirred solution of disuccinimidyl suberate (0.223 g, 0.61 mmol) in DMF (1 mL). The reaction mixture was stirred overnight, concentrated and purified by flash column chromatography eluting with 30% acetonitrile/CH_2Cl_2 provided 0.120 g (46%) of oily material, compound 4. ESMS *m*/*z*: 911.3 $(M + H)^+$.

(((2S)-6-(N-(4-Bromobenzyl)-6-(3-(4-((1,4,7,10-tetrakis(2-amino-2-oxoethyl)-1,4,7,10-tetraazacyclododecan-2-yl)methyl)phenyl)thioureido)hexanamido)-1-hydroxyhexan-2-yl)carbamoyl)-L-glutamic acid (L4). L4 was synthesized following a scheme as shown in Fig. 2B. A mixture of 6-(Boc-amino)hexanoic acid (0.09 g, 0.40 mmol), TSTU (0.121 g, 0.40 mmol) and DIPEA (0.103 g, 0.80 mmol) were stirred in DMF (1 mL) at RT for 1 h. Compound 5 (0.264 g, 0.40 mmol) was added dropwise after dilution with DMF (1 mL). The reaction mixture was stirred for 4 h, concentrated and purified by C_{18} column chromatography eluting with 100% acetonitrile (in 0.1% TFA) provided 0.151 g (44%) of oily material. ^1H NMR (500 MHz, DMSO-*d*6) δ ppm 7.95 (s, 1H), 7.40 (d, *J* = 10 Hz, 1H), 7.34 (d, *J* = 10 Hz, 1H), 7.24 (s, 1H), 7.04 (d, *J* =

5 Hz, 1H), 6.97 (d, *J* = 10 Hz, 1H), 5.48-5.44 (m, 1H), 4.87-4.83 (m, 1H), 4.48-4.36 (m, 2H), 4.26-4.21 (m, 2H), 3.66-3.63 (m, 1H), 3.12-2.95 (m, 4H), 2.90 (s, 1H), 2.81 (s, 1H), 2.73 (s, 2H), 2.33-2.27 (s, 1H), 2.26-2.23 (m, 3H), 2.00-1.98 (m, 1H), 1.77 (m, 1H), 1.66-1.60 (m, 2H), 1.37 (s, 36H), 1.26-1.07 (m, 2H); ESMS *m*/*z*: 843.1 $(M + H)^+$. A cold solution of 50% TFA/CH_2Cl_2 (2 mL) was added to that oily material (0.145 g, 0.17 mmol) and stirred at RT for 2 h. The reaction mixture was concentrated and purified by C_{18} column chromatography eluting with 40% acetonitrile/water (0.1 % TFA in each) and lyophilized to provide 0.067 g (67%) of white solid product as compound 8. ^{1}H NMR (500 MHz, DMSO-*d*6) δ ppm 7.55 (d, *J* = 5.0 Hz, 1H), 7.48 (d, *J* = 5.0 Hz, 1H), 7.19-7.15 (m, 2H), 4.62-4.53 (m, 2H), 4.33-4.27 (m, 2H), 3.40 (s, 1H), 2.98-2.92 (m, 2H), 2.83 (s, 1H), 2.56 (s, 1H), 2.44 (s, 3H), 2.16 (bs, 1H), 1.93-1.84 (m, 2H), 1.74 (s, 2H), 1.67-1.60 (m, 5H), 1.41-1.40 (m, 2H); ESMS *m*/*z*: 574.1 $(M + H)^+$. A reaction mixture of TCMC-Bn-SCN (0.101 g, 0.12 mmol in 200 µL DMSO), 8 (0.069 g, 0.08 mmol in 100 µL DMSO) and DIPEA (0.102 g, 0.79 mmol) were stirred at RT for 3 h. The reaction mixture was concentrated and purified by HPLC to provide the desired ligand L4.

(14S,18S)-9-(4-Bromobenzyl)-2,8,16-trioxo-1-(4,7,10-tris(carboxymethyl)-1,4,7,10-tetraazacyclododecan-1-yl)-3,9,15,17-tetraazaicosane-14,18,20-tricarboxylic acid (L5).

L5 was synthesized following the same scheme as used for L4, shown in Fig. 2B. A mixture of Boc-5-amino valeric acid (0.087 g, 0.40 mmol), TSTU (0.121 g, 0.40 mmol) and DIPEA (0.103 g, 0.80 mmol) were stirred in DMF (1 mL) at RT for 1 h. Compound 5 (0.264 g, 0.40 mmol) was added dropwise after dilution with DMF (1 mL). The reaction mixture was stirred for 4 h, concentrated and purified by C_{18} column chromatography eluting with 100% acetonitrile (in 0.1% TFA) provided 0.151 g (44%) of oily material. ESMS *m*/*z*: 828.1 (M + H). A cold solution of 50% TFA/CH_2Cl_2 (2 mL) was added to the oily material (0.14 g, 0.17 mmol) and stirred at RT for 2 h. The reaction mixture was concentrated and purified by C_{18} column chromatography eluting with 40% acetonitrile/water (0.1 % TFA in each) and lyophilized to provide 0.06 g of white solid

product as compound 9. ESMS *m*/*z*: 560.5 $(M + H)^+$. A reaction mixture of DOTA-NHS-ester (0.090 g, 0.12 mmol in 200 µL DMSO), 9 (0.069 g, 0.08 mmol in 100 µL DMSO) and DIPEA (0.102 g, 0.79 mmol) were stirred at RT for 3 h. The reaction mixture was concentrated and purified by HPLC to provide the desired ligand L5.

Dosimetry translation from murine biodistribution data to human

Dosimetry method. The pre-clinical biodistribution data $([\%ID/g]_M)$ were translated into human whole-organ biodistribution data $([\%ID/organ]_H)$ based on same organ activity concentration to whole-body mass ratio being equal in both species.

$$\left[\frac{\%ID}{organ}\right]_H = \left[\frac{\%ID}{g}\right]_M \cdot TBW_M \cdot \frac{OW_H}{TBW_H} \qquad \text{Eq.1}$$

Where TBW_M [g] is the total body weight of a mouse (25 g) and TBW_H [kg] is that of an adult male human (73.7 kg), and OW_H [kg] is the average male organ weight. The time integrated activity coefficients (TIACs) were calculated for the human adult male organs and used as input into OLINDA/EXM version 1.0 to calculate the clinical ADCs, for the tumor calculations the OLINDA/EXM version 1 sphere model was used for a 1 gram sphere (*1*).

REFERENCES CITED

1. Stabin MG, Sparks RB, Crowe E. OLINDA/EXM: the second-generation personal computer software for internal dose assessment in nuclear medicine. *J Nucl Med.* 2005;46:1023-1027.

2. Banerjee SR, Foss CA, Pullambhatla M, et al. Preclinical evaluation of ^{86}Y-labeled inhibitors of prostate-specific membrane antigen for dosimetry estimates. *J Nucl Med.* 2015;56:628-634.

3. Banerjee SR, Kumar V, Lisok A, et al. ^{177}Lu-Labeled Low-Molecular-Weight Agents for PSMA-Targeted Radiopharmaceutical Therapy. *Eur J Nucl Med Mol imaging.* 2019.

4. Banerjee SR, Pullambhatla M, Byun Y, et al. Sequential SPECT and optical imaging of experimental models of prostate cancer with a dual modality inhibitor of the prostate-specific membrane antigen. *Angew Chem Int Ed.* 2011;50:9167-9170.

5. Tykvart J, Schimer J, Barinkova J, et al. Rational design of urea-based glutamate carboxypeptidase II (GCPII) inhibitors as versatile tools for specific drug targeting and delivery. *Bioorg Med Chem.* 2014;22:4099-4108.